A volumetric technique for fossil body mass estimation applied to *Australopithecus afarensis*

Charlotte A. Brassey[a, *, +], Thomas O'Mahoney[b, +], Andrew T. Chamberlain[b], William I. Sellers[b]

[a]School of Science and the Environment, Manchester Metropolitan University, Chester Street, Manchester, M1 5GD, UK

[b]School of Earth and Environmental Sciences, University of Manchester, Oxford Road, Manchester, M13 9PT, UK

[*]Corresponding author; c.brassey@mmu.ac.uk

[+]These authors contributed equally to this work

Keywords: Lucy; reconstruction; convex hull; hominin; primate;

Abstract

Fossil body mass estimation is a wellestablished practice within the field of physical anthropology. Previous studies have relied upon traditional allometric approaches, in which the relationship between one/several skeletal dimensions and body mass in a range of modern taxa is used in a predictive capacity. The lack of relatively complete skeletons has thus far limited the potential application of alternative mass estimation techniques, such as volumetric reconstruction, to fossil hominins. Yet across vertebrate palaeontology more broadly, novel volumetric approaches are resulting in predicted values for fossil body mass very different to those estimated by traditional allometry. Here we present a new digital reconstruction of *Australopithecus afarensis* (A.L. 288-1; 'Lucy') and a convex hull-based volumetric estimate of body mass. The technique relies upon identifying a predictable relationship between the 'shrink-wrapped' volume of the skeleton and known body mass in a range of modern taxa, and subsequent application to an articulated model of the fossil taxa of interest. Our calibration dataset comprises whole body computed tomography (CT) scans of 15 species of modern primate. The resulting predictive model is characterized by a high correlation coefficient ($r^2 = 0.988$) and a percentage standard error of 20%, and performs well when applied to modern individuals of known body mass. Application of the convex hull technique to *A. afarensis* results in a relatively low body mass estimate of 20.4 kg (95% prediction interval 13.5–30.9 kg). A sensitivity analysis on the articulation of the chest region highlights the sensitivity of our approach to the reconstruction of the trunk, and the incomplete nature of the preserved ribcage may explain the low values for predicted body mass here. We suggest that the heaviest of previous estimates would require the thorax to be expanded to an unlikely extent, yet this can only be properly tested when more complete fossils are available.

Introduction

Body mass is a critical constraint on an organism's ecology, physiology, and biomechanics, and is a required input parameter in many ecological and functional analyses. For paleontologists, it is thus highly desirable to reconstruct body mass for fossil species. Indeed, important studies concerning the evolution of brain size (McHenry, 1976), locomotor kinematics (Polk, 2004), and energetics (Steudel-Numbers, 2006) in hominins have all required reliable fossil body mass estimates.

The fossil record is, however, extremely fragmentary and the majority of specimens are known only from isolated elements. For this reason, the most common approach to mass estimation exploits a tight correlation between body mass and a given skeletal dimension or dimensions in a modern calibration dataset to derive a predictive equation. Within the field of physical anthropology, cranial metrics have been used in a predictive capacity, including orbital area (Kappelman, 1996), orbital height (Aiello and Wood, 1994), and facial breadth (Spocter and Manger, 2007). However, far more common are mass prediction equations based on postcranial elements, which Auerbach and Ruff (2004) subdivide into 'mechanical' and 'morphometric' methods on the basis of the chosen skeletal element. Mechanical techniques employ postcranial, mass supporting structures as a basis for predictive equations, including knee breadth (Squyres and Ruff, 2015), vertebral centrum area (McHenry, 1976), femoral head and neck breadth (Ruff et al., 1991), and humeral and radial head diameter (McHenry, 1992). Alternatively, morphometric techniques reconstruct fossil mass based on the direct assessment of body size and shape. For example, a series of studies (Ruff, 1994, 2000; Ruff et al., 2005) have found the combination of stature and biiliac breadth to provide relatively accurate estimates of body mass when applied to modern humans. Footprint area (as measured from fossil trackways) has even been used as a means of reconstructing hominin body mass (Dingwall et al., 2013, Masao et al., 2016).

Whilst bivariate and multivariate mass predictive equations benefit from their applicability to fragmentary material and the ability to generate large modern comparative datasets, there

are associated disadvantages: which skeletal element to use, extrapolation, biasing by robust/gracile elements, and mass and inertia properties.

Which skeletal element to use?

When numerous skeletal elements are available for a particular fossil individual, it may be unclear which bony dimension ought to be used as a basis for mass prediction. If both a complete femur and tibia are available, for example, either could be considered a suitable mass-supporting structure upon which to base a fossil mass estimate. Yet previous research estimating body mass for non-primate fossil mammals demonstrates that estimates can span two orders of magnitude for the same individual depending on which limb bone or skeletal metric was used for prediction (Fariña et al., 1998). This example includes unusually proportioned mammals such as xenarthrans, and mass estimates for fossil hominins are not known to vary to such a degree (e.g., McHenry's 1992 estimates for the *Australopithecus afarensis* skeleton A.L. 288-1 based on different anatomical parts range between 11.8 and 37.1 kg). However, McHenry and Berger (1998) do highlight the potential for hominin mass estimates to vary considerably depending upon the use of forelimb or hind limb joint size as the basis for the predictive equation. Ultimately, a decision must still be made on which equation to use, taking into account the predictive power of the model (r^2 or percentage prediction error) and the existence of taphonomic damage or unusual morphology, for example, that may otherwise bias the result.

Extrapolation

Whilst typically less extreme in paleoanthropology compared to other disciplines of vertebrate paleontology, body mass estimations are often conducted on fossil specimens lying outside the range of body sizes occupied by the modern calibration dataset. Potential dwarfism (Brown et al., 2004, Vančata, 2005, Holliday and Fransiscus, 2009, Stein et al., 2010; Herridge and Lister, 2012) and gigantism (Millien and Bovy, 2010; Bates et al., 2015) are recurrent themes for fossil mass reconstructions, yet by their very nature they require an

97 extrapolation of a predictive relationship beyond the modern range. In such instances,
98 extrapolated predictions should be regarded as extremely speculative (Smith, 2002) due to a
99 lack of evidence that the linear model holds beyond the extant dataset and a rapid widening
100 of confidence intervals around the prediction.
101
102 *Biasing by robust/gracile elements*
103 Underlying the theory of bivariate/multivariate mass prediction is the assumption that the
104 relationship between mass and a given skeletal dimension identified in modern species also
105 holds for the fossil species of interest. In some instances, however, we can intuitively
106 appreciate that species may be characterized by unusually proportioned skeletal elements
107 (the elongated canines of sabretoothed cats, or the robust hind limb bones of some
108 dinornithiform birds for example). When placed into the context of the rest of the body, such
109 enlarged/reduced features are obvious. Should such structures be used as a basis for mass
110 estimation, however, unfeasibly large/small fossil species will be reconstructed (Braddy et
111 al., 2008 vs. Kaiser and Klok, 2008, Brassey et al., 2013). This is a particular concern when
112 dealing with isolated elements in the absence of complete skeletons, where relative
113 robustness/gracility cannot be known. In physical anthropology, for example, the mass
114 estimation of *Gigantopithecus* on the basis of molar size (Conroy, 1987) or mandible size
115 (Fleagle, 2013) is vulnerable to this problem.
116
117 *Mass and inertia properties*
118 Currently, traditional allometric predictive relationships produce a solely scalar value for
119 body mass (i.e., X species weighed Y kg). Whilst these single values may be of use in
120 subsequent ecological analyses or evolutionary models, they are not informative with
121 regards to how said mass is distributed around the body. Inertial properties (including mass,
122 center of mass, and moments of inertia) are essential when conducting biomechanical
123 simulations such as multibody dynamic analyses of locomotion and feeding. Previous
124 biomechanical analyses of fossil hominins have therefore reconstructed inertial parameters

on the basis of modern human and chimpanzee values (Crompton et al., 1998; Kramer and Eck, 2000; Sellers et al., 2004), due to a lack of viable alternatives.

Volumetric techniques

For the above reasons, volumetric mass estimation techniques have become increasingly popular within the field of vertebrate paleontology (see Brassey, 2017 and references therein). Historically, volume based estimates required the sculpting of scale models and the estimation of volume via fluid displacement (Gregory, 1905; Colbert, 1962; Alexander, 1985). However, as part of the recent shift towards 'virtual paleontology' (Sutton et al., 2014; as characterized by the increased application of digital imaging techniques such as computed tomography, laser scanning, and photogrammetry), three-dimensional (3D) computational modeling of fossil species is becoming increasingly common. As articulated skeletons are digitized faster and with greater accuracy, volumetric mass estimation techniques now involve the fitting of simple geometric shapes (Gunga et al., 1995, 1999) or more complex contoured surfaces (Hutchinson et al., 2007; Bates et al., 2009) to digital skeletal models within CAD (computer-aided design) packages. Volumetric approaches overcome many of the limitations associated with traditional allometric mass estimation methods, including the need to extrapolate predictive models and rely upon single elements, whilst also allowing inertial properties to be calculated if desired.

Both physical sculpting and digital CAD 'sculpting' of 3D models inevitably involves some degree of artistic interpretation, however. By attempting to reconstruct the external appearance of an extinct species, assumptions must be made regarding the volume and distribution of soft tissues beyond the extent of the skeleton. Whilst those undertaking said modeling necessarily rely upon their experience as anatomists to inform reconstructions, previous research has found resulting mass estimates to be sensitive to the individual carrying out the procedure (Hutchinson et al., 2011). The convex hulling technique applied in the present paper was therefore developed with the aim of incorporating many of the benefits associated with volumetric mass estimation, whilst overcoming the subjectivity inherent in 'sculpted' models (Sellers et al., 2012).

153 A convex hull is a geometric construct commonly used within mathematical sciences.
154 The convex hull of *n* points is simply the minimum size convex polytope that still contains *n*
155 (Fig. 1). In two dimensions, the process is analogous to stretching an elastic band around
156 the series of points, with the band 'snapping-to' the outermost points. The ultimate form of
157 the hull is dictated by a small number of points lying at the extremities and for a given set of
158 points there is a unique convex hull. Two-dimensional (2D) convex hulls have often been
159 applied in ecology as a means of defining the range size of wild animals (Harris et al., 1990
160 and references therein) or quantifying population niche width around stable isotopic data
161 (Syväranta et al., 2013). A 3D convex hull can, likewise, be fitted to a suite of x, y, z
162 coordinates to form a tight-fitting 3D polyhedron (Fig. 2). Three-dimensional convex hulls are
163 more commonly applied within the fields of robotics and computer games design to rapidly
164 detect potential collisions between objects (Jiménez et al., 2001), but have also been
165 applied in the biological sciences to estimate volume of crop yield (Herrero-Huerta et al.,
166 2015) or canopy foliage (Cheein and Guivant, 2014).
167 Sellers et al. (2012) initially developed the convex hull mass prediction technique on
168 a dataset of modern quadrupedal mammals. Using a LiDAR (light detection and range)
169 scanner, the articulated skeletons of 14 mammals located within the main gallery of the
170 Oxford University Museum of Natural History (OUMNH) were digitized. Point clouds
171 corresponding to individual skeletons were isolated from the larger gallery scan and each
172 skeleton subdivided into functional units (e.g., head, neck, thigh, shank, and trunk). Convex
173 hulls were fitted to the point clouds representing all functional units, and the total convex hull
174 volume of the skeleton was calculated as the sum of individual segments (Fig. 2). Total
175 convex hull volume was subsequently multiplied by a literature value for body density to
176 produce a convex hull mass and regressed against body mass to produce a linear bivariate
177 predictive equation. The model was characterized by a high correlation coefficient and
178 percentage standard error of the estimate (%SEE) of approximately 20%.
179 In some respects, convex hulling is a hybrid technique, combining volumetric data
180 from an articulated skeletal model with the more traditional allometric mass estimation

approach. By incorporating data from the entire skeleton, the technique may be less sensitive to particularly robust or gracile elements than previous approaches, and no decision need be made regarding which particular bone to base estimates upon. As a volumetric technique, convex hulling may also provide values for segment inertial properties whilst avoiding the subjectivity inherent within previous sculpting techniques. The initial Sellers et al. (2012) application of convex hulling did, however, require a literature value for body density to be assigned to the modern dataset, which was itself heavily dominated by ungulates.

Subsequent applications of the convex hulling procedure have sought to overcome some of the above concerns. Brassey et al. (2014) directly regressed convex hull volume against body mass to generate scaling equations for both mammals (including primates) and birds, without the requirement to assign a literature value for body density. There is an inherent assumption, however, that the body density of the fossil species falls within the range of values occupied by the modern taxa. Furthermore, Brassey et al. (2013, 2016) produced additional convex hull predictive equations based upon modern ratites and pigeons for application to the mass estimation of the extinct moa and dodo, respectively.

Mass estimation of Australopithecus afarensis *(A.L. 288-1)*

The partial *Australopithecus afarensis* skeleton A.L. 288-1 ('Lucy') is one of the most complete Pliocene hominin skeletons found to date, with over 40% of the skeleton preserved, including the pelvis and most of the upper and lower limbs represented by at least one side (Johansen and Edey, 1981; Johanson et al., 1982). The only other *A. afarensis* remains approaching such percentage preservation is the Woranso-Mille specimen (Haile Selassie et al., 2010), with other relatively complete specimens including the *Australopithecus sediba* remains from Malapa (Berger et al., 2010) and the 'Little Foot' skeleton, attributed to *Australopithecus prometheus* (Clarke, 1998). Unsurprisingly, A.L. 288-1 has therefore been subject to a wealth of mass estimation studies spanning the last 35 years (Fig. 3).

Due to the relative completeness of the specimen, previous mass estimates of A.L. 288-1 have been based upon axial, sacral, forelimb, and hind limb elements, and indeed multivariate models incorporating several elements. Table 1 details the results of McHenry's (1992) often-cited study, in which the body mass of A.L. 288-1 was estimated on the basis of several skeletal elements using both an ape- and human-based predictive equation. As can be seen in Table 1, estimated body mass ranged between 13 and 37 kg within a single study (based on the radial head and femoral shaft respectively). More broadly, across the gamut of previous mass estimates for A.L. 288-1(including predictive intervals when calculated), published values range from 13 to 42 kg (Fig. 3), with studies diverging in their choice of reference dataset, skeletal metric, and Type I versus Type II regressions. It should be noted, however, that the mass estimates in Figure 3 represent the extreme upper and lower values of each publication and do not account for any author preference stated with regards to which estimate is most appropriate. McHenry (1992) favors the human-based predictive equation for example, narrowing the range to 17–37 kg. Likewise, Squires and Ruff (2015) present results from both Type I and Type II regressions, but consider the results of the ordinary least squares (OLS) analysis inappropriate and favor reduced major axis (RMA). Yet despite three decades' worth of debate regarding the appropriate choice of skeletal element, dimension, modern calibration dataset, and regression type, Figure 3 suggests most studies do indeed overlap in the area of 25–37 kg.

Although A.L. 288-1 has frequently been the subject of fossil hominin mass prediction studies, a volumetric reconstruction has never been attempted. Numerous dynamic analyses of locomotion in *A. afarensis* have required values for center of mass and segment inertial properties for the specimen (Crompton et al., 1998; Kramer, 1999; Kramer and Eck, 2000; Sellers et al., 2004; Wang et al., 2004; Nagano et al., 2005; Sellers et al., 2005). In all instances, however, body mass has been assigned a priori on the basis of previously published estimates, with the mass subsequently distributed around the skeleton via scaling of human and/or chimpanzee inertial properties. The slow adoption of volumetric mass estimation in physical anthropology compared to other paleontological disciplines

(Brassey et al., 2017) may be attributed partly to the relative paucity of complete skeletons. Whilst A.L. 288-1 is indeed one of the most complete Pliocene hominins ever found, large portions of the skeleton were not recovered. Most notably, the vertebral column and shoulder girdle is poorly represented, with considerable portions missing. The rib cage is relatively well represented, with material available for all ribs barring ribs 2 and 12. Due to the fragmentary nature of the costal remains, a good deal of reconstruction and interpolation is required however. This is particularly problematic when conducting volumetric mass estimation, as the vast majority of total body volume resides within the trunk.

A volumetric reconstruction of *A. afarensis* A.L. 288-1 is a worthwhile endeavor on several grounds. Recent studies of non-hominin fossil skeletons have found traditional bivariate mass predictions to be unfeasibly high (Brassey et al., 2013; Bates et al., 2015), but such insight may only be gained via attempting to fit volumetric shapes around the skeleton to simulate the extent of soft tissue required to achieve said mass values. Whilst the wealth of pre-existing mass estimates of A.L. 288-1 is commendable, they are heavily skewed towards hind limb and pelvis based regressions. Although this may be justifiable on mechanical grounds, it would seem prudent to also approach the problem of mass estimation from an alternative and innovative direction incorporating information from across all available skeletal material.

As a volumetric technique, convex hulling is well suited to the reconstruction of specimens characterized by incomplete thoracic material. The extent of an object's convex hull is dictated by its geometric extremes (Fig. 1), ensuring the presence of 'missing data' within the bounds of the hull does not impact upon its ultimate volume. As such, absence of or damage to vertebrae or ribs lying within the bounds of the 'trunk' functional unit will not negatively impact resulting mass estimates. A corollary, however, is this makes it even more essential that the placement of geometric extremes (and any additional spacing to account for missing elements) is reliable.

In this paper, we use convex hulling to estimate the body mass of the (reconstructed) A.L. 288-1 skeleton. In doing so, we also explore the effect of uncertainty in the articulation

of the thorax and reconstruction of the pelvis on resulting mass estimates. In the past, the form of the *A. afarensis* ribcage has been debated, typically falling into a dichotomy of an ape-like 'funnel shape' versus human-like 'barrel shape' (Latimer et al., 2016 and references therein). Despite this interest, relatively little is known of the effect thoracic morphology may have upon resulting mass estimates and inertial properties. The novel application of convex hulling to the mass estimation of *A. afarensis* will act as an independent check on the validity of previous allometry based mass predictions and going forward will further inform discussions on the nature of australopith locomotion and sexual dimorphism that are themselves heavily reliant upon values for body mass.

Here, we choose to focus on just one hominin specimen as a case study of the convex hulling methodology. In doing so, we accompany our mass estimates with the most transparent and rigorous 3D reconstruction of A.L. 288-1 to date. We aim to equip the reader with the methodological tools necessary to expand this technique, as well as a grounding in its current benefits and limitations. Given the ongoing discovery of exceptional specimens and the rapidly declining costs of digitization, we are optimistic that this technique can be more broadly applied within the field of human evolution. Of course, this will be facilitated by a shift towards authors making underlying digital datasets freely available (Davies et al., 2017), a practice from which we all stand to benefit greatly.

Materials and methods

Modern calibration dataset

There is considerable debate in the literature regarding the appropriate choice of reference population when applying predictive equations to fossil hominins. Typically, calibration datasets comprise modern humans, modern human populations of small stature, African great apes, (Jungers, 1990; Hens et al., 2000; Grabowski et al., 2015) or a combination of the above. When deriving mass prediction equations based on hind limb dimensions, human based models are often preferred due to a perceived similarity in limb function, i.e., potential bipedalism. This, in itself, requires an a priori assumption of the fossil

taxa being bipedal, an issue that is particularly problematic should the derived body mass subsequently be used in biomechanical analysis of potential bipedalism. Alternatively, a training dataset comprising modern human populations of small stature might be preferred to minimize the degree of extrapolation necessary from smallest modern individual to fossil taxa. But again, this involves an assumption of fossil hominin body size (i.e., lying below that of most modern individuals) prior to the analysis (Konigsberg et al., 1998).

Given the paucity of available whole body CT data, a convex hull predictive model based solely on modern humans is currently difficult to achieve, particularly in the case of humans from small-stature populations. Here, we apply an 'all primate' predictive model to the estimation of *A. afarensis* body mass. In doing so, we make no assumptions regarding the locomotor function of the hind limbs or the range of body sizes probably occupied by *A. afarensis.* By applying an 'all primate' model, we assume there is a consistent relationship between the volume defined by the extremities of the skeleton and total body mass. As an alternative way of conceptualizing this, we assume the volume (and density) of soft tissue distributed outside the bounds of the convex hull to scale to body mass in a predictable manner across all primates, including fossil hominins. As such, the convex hull is conceptually closer to a 'morphometric' rather than 'mechanical' technique as defined by Auerbach and Ruff (2004).

Computed tomography The extant dataset comprises 15 species of modern primate (Table 2), several of which were included in an initial convex hulling study on extant mammals (Brassey et al., 2014). CT scans of whole carcasses were sourced from the Kyoto University Primate Research Institute (KUPRI, http://dmm3.pri.kyoto-u.ac.jp) and the male human from the Visible Human Project (National Library of Medicine, NLM, www.nlm.nih.gov/research/visible). In the absence of available whole body CT scans from other ethnic groups, the human representative is a non-pathological, white male. Additional carcasses were sourced from the National Museum of Scotland (NMS) and were CT scanned at the University of Liverpool using a Toshiba Aquilion PRIME helical veterinary

scanner. Slice thickness ranged between 0.5 and 2.7 mm with pixel spacing of 0.29–0.98 mm/pixel, depending on the total size of the animal.

CT scans were imported in OsiriX (Rosset et al., 2004) and isosurfaces of whole articulated skeletons thresholded out on the basis of grayscale values (Fig. 2) and exported as OBJ files. In some instances, cadavers have been subject to postmortem investigations, including the detachment of portions of the cranial vault or sternum. In those cases, the 3D model of the skeleton was digitally repaired and the removed elements realigned and rearticulated in 3ds Max (www.autodesk.com). Skeletal models were subsequently imported into Geomagic Studio (3D Systems, USA) and segmented into functional units (such as head, neck, thigh, trunk; Fig. 2). When present, tails were further subdivided to ensure tight fitting hulls. Individual body segments were saved as OBJ files and convex hulls fitted around the segments using the 'convhulln' function of MATLAB (Mathworks, USA), which implements the qhull algorithm to find the convex hull and return its enclosed volume in minimal computer time (Barber et al., 1996).

Statistical analysis Total convex hull volume (m^3) for each skeleton was calculated as the sum of individual segment volumes. Total convex hull volume was then regressed against known body mass (kg) following $\log_{10}$ transformation in R (R Core Team, 2014). In two instances, associated body masses were not available (*Pan troglodytes, Hylobates lar*) and were therefore estimated using a pre-existing bivariate equation based upon radial head surface area in extant hominoids (Ruff, 2003). The effect of including these individuals in the regression analysis is discussed further in the results section. Additionally, several individuals sourced from NMS had, upon inspection of the CT data, been subject to some degree of postmortem surgery in the region of the abdomen, which may have resulted in removal of gut contents and certainly fluid loss. Given that the exact nature of these procedures is unknown, it is not possible to accurately correct cadaveric body mass for these losses. Rather, the regression analyses were rerun excluding these individuals, and the impact on the predictive model is discussed further below.

Ordinary least squares (OLS) was preferred in this instance, as Type-I regressions are recommended when used in a predictive capacity (Smith, 2009), however, results using reduced major axis (RMA) are also included for reference. In addition, a phylogenetic generalized least squares (PGLS) regression was applied to account for the evolutionary non-independence of data points. A consensus phylogeny of primates was downloaded from the 10kTrees website (Arnold et al., 2010) and PGLS analyses conducted in MATLAB using the 'Regressionv2.m' program (Lavin et al., 2008). Raw CT scans of NMS sourced primates have been made available by the authors on figshare (DOI: 10.6084/m9.figshare.c.3462618), whilst KUPRI-sourced scans can be accessed online via the Digital Morphology Museum (http://dmm3.pri.kyoto-u.ac.jp) and access to the human dataset can be requested from the Visible Human Project (www.nlm.nih.gov/research/visible).

In addition to the primate carcasses included in the original regression model, supplementary modern specimens of known body mass were subjected to the predictive model in order to test its performance. Six primate scans were sourced from KUPRI, and an additional six CT scans of human males were taken from the National Cancer Imaging Archive (NCIA; Clark et al., 2013; www.cancerimagingarchive.net). The additional CT scans were segmented and processed as above and convex hull based body mass estimates derived using the OLS equation. Furthermore, a "leave-one-out" jackknife analysis of the regression model was conducted, in which one specimen in turn from the original calibration equation was removed and subjected to mass estimation on the basis of the remaining dataset.

Application to fossil material

Casts of the *A. afarensis* partial skeleton A.L. 288-1 were surface scanned using an LMI HDiR3 Advance structured light scanner (LMI technologies, Delta, BC) at a resolution of approximately 50 μm. At the time of initial analysis, no μCT data or associated models were publicly available. Subsequently, models of the humerus, scapula fragment, proximal tibia,

and distal femur have been made available from http://www.elucy.org. A deviation analysis of our casts against models based upon said μCT data has shown minimal difference between reconstructions (see Supplementary Online Material [SOM] Figure S1). As such, it was decided to proceed with a model composed predominantly of casts, with the exception of those elements made publicly available by Kappelman et al. (2016) at elucy.org. All 'sculpts' were constructed from modelling clay by ATC filling in missing parts of casts without replacing existing cast material. This reconstruction therefore functions as a working hypothesis until access to μCT data of the entire skeleton is freely available. All modern human data referred to here are clinical CT scans from the NCIA, specifically females from the Cetumixab drug trial and *Pan troglodytes* CT scans from the Arizona primate foundation's skeletal collection (digitized and curated at http://www.carta-anthropogeny.org), with full details of the specimens employed provided in SOM Table S1.

Pelvic region The sacrum is crushed, particularly on the left side, and the model was therefore virtually cut in half and the right side mirrored following the protocol outlined in Zollikofer and Ponce de León (2005) and Gunz et al. (2009). In doing so, much of the original distortion was removed, resulting in a marginally wider sacrum than previous reconstructions of Tague and Lovejoy (1986) and Schmid (1983). The complete left os coxa is crushed in the region of the sacroiliac joint and distorted in the ischiopubic region (Johanson et al., 1982). The scanned model was virtually cut into its constituent parts and rearticulated with a concentration on the internal arc being consistent. The complete left os coxa was then articulated to the sacrum with a midline projected from the sacrum, as well as two lines either side at 6 mm apart to model the length of the ligament for the pubic symphysis. This distance is based on measurements of a small mixed sample of *Homo sapiens (n* = 8*)* and *Pan troglodytes* (*n* = 6) medical scans of the pelvic area, where average distance between pubic symphyses was 5.7 mm with a standard deviation of ~1 mm. Given that there is definitely crushing of the sacroiliac joint in AL288-1 (Johanson et al., 1982;

Williams and Russo 2016, Williams and Russo, 2016), the alignment allows for the eventual restoration of the true joint, as there is also space between our reconstructed sacrum and the pubic symphysis. The resulting articulation of the right os coxa was then mirror-imaged using the midline plane of the sacrum as the reflection plane. The complete pelvis and associated linear metrics can be found in Figure 4, and Tables 3 and 4. A complete 3D model suitable for rapid prototyping is available as supplementary data on Figshare (DOI: 10.6084/m9.figshare.c.3462618, alongside a figure illustrating the reconstruction stages.

Lower limb The left femur is mostly complete, although the distal epiphysis of the original cast was misaligned. The distal epiphysis was therefore virtually rearticulated, along with the proximal fragment that includes the femoral neck and most of the head, to complete the element, ensuring that the dimensions of our scans matched those of the original fossil (Johansen et al., 1982). The length of the incomplete left tibia was estimated using the tibial:humeral ratio of the Woranso-Mille specimen (Haile Selassie et al., 2010; Haile Selassie and Su, 2016) as a reference, whilst the missing diaphyseal material was not reconstructed, as this has no bearing upon the convex hull volume. The fibula was reconstructed by scanning a physical sculpt constructed by ATC, incorporating the cast of the well preserved distal portion of the fibula (A.L. 288-1at), proportioned to match our estimated tibial length and articulating anatomically with the tibia proximally and the talus distally. In the foot, the A.L. 288-1 talus was used to scale a scan of a reconstruction of the OH 8 right foot in which missing components (principally the phalanges) were sculpted by ATC to the proportions of a modern human foot. The lengths of all reconstructed limb bones are presented in Table 5.

Upper limb The right scapula preserves the glenoid in its entirety and part of the spine and the base of the acromial process. The missing morphology was reconstructed through a thin plate spline morph of the modern human reference sample (SOM Table S1) through geometric morphometric analysis of 20 type I and II landmarks and 20 curve semilandmarks.

All landmark data are available as supplementary data on Figshare (DOI: 10.6084/m9.figshare.c.3462618), as is our reconstructed scapula model. The resulting morphed model was then mirrored to produce a left scapula. A scan of the complete *A. sediba* right clavicle (UW88-38) (http://www.morphosource.org) was scaled on the basis of a fragment from A.L. 288-1 and also mirrored. The right humerus was based on the recent reconstruction of Kappelman et al. (2016) and mirrored in place of the left.

A.L. 288-1 has well preserved left and right side proximal and distal ulnae (Johanson et al., 1982) but on both sides regions of the midshaft are missing, necessitating estimation of maximum length and longitudinal curvature. We reconstructed the missing parts of the shaft in modeling clay after arranging the preserved parts in approximate anatomical alignment, utilizing the ulnar maximum length estimation (from proximal to distal extremities excluding the styloid process) of 220 mm (Kimbel et al., 1994) and longitudinal curvature of 2 mm (left) and 4 mm (right) in accordance with the estimates of Drapeau et al. (2005:Table 4).

The proximal, midshaft, and distal fragments of the right radius were aligned and spaced using the proximal and distal articulations between the radius and the reconstructed right ulna as a guide. The resulting maximum length of 204 mm is almost identical to the value of 203 mm (95% confidence interval [C.I.] ± 29 mm) published by Asfaw et al. (1999). As with the ulna, we have reconstructed the radius with slight longitudinal curvature.

Only the left capitate (A.L. 288-1w) and an unsided non-pollical proximal phalanx (A.L. 288-1x) are preserved from the A.L. 288-1 hand. The dimensions of the capitate and of the distal articular surface of the radius in A.L. 288-1, together with the metacarpal/ulna length ratio and the metacarpal/phalangeal length ratios in other *A. afarensis* material (Bush et al., 1982; Alba et al., 2003; Drapeau et al., 2005), place some constraints on the size and shape of the hand in A.L. 288-1. A human hand obtained from the NCIA sample was scaled to fit the A.L. 288-1w capitate and our estimates of second and third metacarpal lengths.

459 Vertebral column The specimens A.L. 288-1ae, A.L. 288-1af, A.L. 288-1ad, A.L. 288-1ac,
460 and A.L. 288-1aa were originally interpreted as the bodies of a probable T6, a probable T8,
461 and T10, T11, and L3 vertebrae, respectively (Johanson et al., 1982). However, a recent
462 revision by Meyer et al. (2015) interpreted these vertebrae as T6, T7, T9, T10, and L3, and
463 we follow this numbering here. The number of lumbar vertebrae originally present in A.L.
464 288-1 has also been debated. Cook et al. (1983) suggested A.L. 288-1 had five lumbar
465 vertebrae, yet Latimer and Ward (1993) observed six lumbar vertebrae in available
466 skeletons of *A. africanus* (see also Robinson, 1972; Sanders, 1998) and argued this number
467 is therefore likely to represent the primitive condition in hominins. They suggest the T13 of
468 hominoids underwent transformation into L1 in hominins as a means of facilitating lumbar
469 lordosis, resulting in Pliocene hominins possessing 12 thoracic and six lumbar vertebrae,
470 and a subsequent reduction to the five lumbar vertebrae typical of Pleistocene and Holocene
471 humans. Subsequent research (Williams et al., 2015, 2016) has argued that this is not
472 correct and that australopiths had five lumbar vertebrae. We concur with this argument and
473 in our reconstruction, A.L. 288-1 has five lumbar vertebrae.
474 Table 6 compares the dimensions of the vertebral bodies in A.L. 288-1 with
475 dimensions taken from vertebral columns from *H. sapiens* (a medieval sample and Andaman
476 Islanders), *P. troglodytes*, and archaic hominins prior to around 1.5 Ma. It can be seen that
477 the ratios of the heights of the surviving thoracic and lumbar vertebrae in AL288-1 are very
478 similar to modern humans, particularly our smaller bodied Andaman sample, but are less
479 similar to *P. troglodytes*. It is also very similar to that of STS-14.
480 Several values for total dry height of the A.L. 288-1 vertebral column (L5-C2) are
481 presented, depending upon the modern reference sample used (Table 7). We prefer the
482 value based mainly on Andaman Islanders for the above reason and, as the maximum
483 length, will reflect an upper limit for total body size. The dry column height for our
484 reconstruction is 339.8 mm, without accounting for intervertebral disc heights. Further
485 adjustment to account for disc spacing based upon Gilad and Nissan (1986) and Kunkel et
486 al. (2011) result in a ‘wet’ height of 422.3 mm. The vertebral column from

Cetumixab0522c0433 was manually segmented in Avizo, and the resulting PLY file was scaled to match this height and to the width of the L3 from A.L. 288-1.

Thorax The subject of the shape of the *Australopithecus* thorax has been one of considerable debate (Schmidt, 1983; Lewin and Foley, 2004; Haile Selassie et al., 2010; Schmid et al., 2013; Latimer et al., 2016;). Both a human 'barrel shape' and hominoid 'funnel shape' ribcage have been proposed for *A. afarensis*, with previous reconstructions being based on very limited fragmentary remains. However, the recent find and subsequent analysis of the Woranso-Mille thoracic remains have supported the *A. afarensis* thorax as being a different form to either of these extremes, with a 'bell shaped' thorax being favored (Latimer et al., 2016). As such, we reconstruct the A.L. 288-1 ribcage using an iterative, geometric morphometric technique based upon a sample of both *H. sapiens* and *P. troglodytes*.

The rib fragments of A.L. 288-1 were positioned using a reference thorax of a modern human scaled to the height obtained above as a guide, purely as a guide for the initial reconstruction. Where appropriate, fossil rib fragments were mirrored to create a starting model based solely on A.L. 288-1 material. The right hand side was preferred as this is generally the better preserved side. Medical CT scans of 10 modern human females were subsequently sourced from the NCIA and 10 *P. troglodyes* from the Arizona Primate Foundation collection (Available from http://www.carta.anthropogeny.org; SOM Table S1). 3D models of the ribcage (or individual ribs in the case of *Pan*) were extracted using the freeware program Stradwin (Treece et al., 1999). For each rib of the modern ribcage dataset, four sets of 61 semilandmarks were placed on the anterior, posterior, cranial, and caudal extremities of the rib head (with up to four fixed landmarks to mark the position of the tubercle and up to four at the head). The semilandmarks were then resampled equidistantly using the R package Morpho (Schlager 2013). Sixty-one semilandmarks were chosen, rather than 15 as employed by Garcia Martinez et al. (2014) in the Kebara reconstruction, as A.L. 288-1's ribs are much more fragmentary. A greater number of landmarks therefore

allows for more of the original fossil data to influence the resulting reconstruction. Semilandmarks missing from each of the A.L. 288-1 ribs were then reconstructed using thin plate splines based upon the entire modern hominoid (i.e., both *H. sapiens* and *P. troglodytes*) reference dataset, in the R package Morpho. Final reconstructed polygon models were created by morphing a chimpanzee rib onto the configuration of predicted landmarks for AL288-1 using the 'warprefmesh' function in Geomorph (version 3.0.3; Adams et al., 2013). Each rib reconstruction was also 3D printed to check its feasibility. The simplified rib heads presented here act only to articulate with the reference spine, and with the exceptions of ribs 7 and 11, have limited biological significance beyond a prediction of overall size. The resulting 3D models were subsequently rearticulated onto the base spine skeletal model. The complete right hand side of the rib cage was mirror-imaged to give the left portion. All landmark data are available as supplementary data on Figshare (DOI: 10.6084/m9.figshare.c.3462618)

Given the fragmentary state of the thorax, ribs 2 and 12 were not included as they are entirely absent from the original. Rib 11 was also not reconstructed in its entirety, as it is extremely variable in length both within and between species (T.O'M., pers obs.), and its curvature does not affect the reconstructed convex hull. As previously stated, a benefit of convex hulling is that the hulls effectively 'snap-to' the outermost points of the region and are therefore insensitive to any missing material within the bounds of the extremities. Furthermore, our attempt to morph a ribcage on the basis of limited thoracic material represents an improvement over previous paleontological reconstructions in which an articulated modern ribcage is simply scaled and substituted into the fossil (Basu et al., 2016). Finally, a modern human sternum from the NCIA sample was scaled to approximately 60% in all directions and articulated with the thorax.

Cranium For the cranium, a scan of the composite *A. afarensis* A.L. 333 reconstruction (available on http://www.morphosource.org) was scaled to fit the existing mandible and cranial vault fragments of A.L. 288-1.

543 The reconstruction of the thorax and final articulated model are illustrated in Figure 5.
544 The overall height of A.L. 288-1 is reconstructed as 1106 mm, and bi-iliac breadth is 264
545 mm. The whole model accompanies the publication as supplementary data on Figshare
546 (DOI: 10.6084/m9.figshare.c.3462618; with the exception of the proximal tibia, reconstructed
547 humerus, and distal femur, which can be obtained from http://www.elucy.org and the
548 clavicle, which can be obtained from http://www.morphosource.org). All landmark datasets
549 used in the model construction are also available, as well as landmarks indicating placement
550 of model files available from elsewhere (SOM Figure S2a,b).
551
552 Sensitivity analysis In volumetric reconstructions, the majority of total volume lies within the
553 trunk. As such, convex hull mass estimates are particularly sensitive to uncertainty in the
554 articulation of this region. As stated above, the height of the model presented here is in
555 broad agreement with previous reconstructions, and we can be relatively confident in the
556 dimensions of the trunk in the superior-inferior direction. However, to quantify the effect of
557 uncertainty in the remaining two dimensions, two additional models were created in which
558 the entire trunk segment (pelvis, ribs, vertebrate, scapula, sternum, and clavicle) were
559 scaled in the dorsoventral and mediolateral directions by 10% and 20%, respectively.
560
561 **Results**
562 *Predictive model*
563 The results of the regression analyses can be seen in Table 8 and Figure 6A. The
564 OLS fit is characterized by a high correlation coefficient (r^2 = 0.988) and a %SEE of 20%,
565 whilst the type-II RMA regression has a %SEE of 14%. When phylogenetic non-
566 independence was taken into account by conducting PGLS, %SEE increased to 26%.
567 Ordinary least squares is typically the preferred regression type when used in a predictive
568 capacity (Smith, 1994; 2009) and is therefore reported throughout. Application of RMA
569 results in very similar predictions (within ~2%) to those generated using OLS.

In two instances, associated body mass was not available for the modern primate cadaver and values were therefore assigned using a pre-existing bivariate equation based upon radial head surface area in extant Hominoids (Ruff, 2003). As such, these values are estimates themselves with associated errors. Regression analyses were therefore rerun excluding these individuals and the results presented in SOM Table S2. Exclusion of these individuals had a negligible effect on the predictive equation, however, and resulting mass estimates deviated by ~5% from the original equation. Likewise, some individuals sourced from the National Museum of Scotland had been subject to postmortems and removal of an unqualifiable mass of gut content. Removal of these individuals also had a very minor impact on the predictive equation (SOM Table S3) and decreased fossil mass estimates by ~2% relative to the original equation.

Application to modern individuals of known body mass

Overall, the original OLS predictive model performed well when applied to modern primate specimens of known body mass. The model performed best when predicting the mass of a male human of normal BMI (21.4), reliably estimating body mass to within 800 g (Table 9). For the night monkey and squirrel monkeys, percentage error on the mass estimates were within the bounds of what would be expected on the basis of a mean absolute prediction error of 13.5% calculated for the OLS predictive equation. However, in the case of the Japanese macaques, prediction error was high (27–29%, Table 9). The "leave-one-out" jackknife analysis resulted in an average prediction error of 14.8%, ranging from 0.5–37.4%.

The predictive equation performed as expected when applied to a sample of human males with varying body mass index (BMI, Fig. 7). Individuals with a BMI falling within the 'healthy' range (18.5–25) had percentage prediction errors between 1–15%, in line with the jackknife analysis above. In individuals characterized as overweight (BMI 25–30) or obese (BMI >30), predicted mass increasingly deviated from known mass, resulting in a prediction error of 32% in one particularly obese individual.

598

599 *Application to A.L. 288-1*

600 Total height of the A.L. 288-1 reconstruction presented here is 1106 mm, which is
601 slightly taller than the widely accepted estimate of 1070 mm by Jungers (1988a). Likewise,
602 reconstructed bi-iliac breadth is 264 mm, which is at the upper end of the range of published
603 estimates of 228–268 mm (Berge and Goularas, 2010; Ruff, 2010). In contrast, bi-iliac
604 breadth of the 10% and 20% expanded models is 290 mm and 317 mm, respectively, which
605 are well above previously published estimates.

606 Fitting convex hulls around the body segments of our 3D reconstruction of *A.*
607 *afarensis* (288-1) resulted in a total convex hull volume of 0.0148 m^3 (Fig. 8, Table 10).
608 Increasing the dorsoventral and mediolateral dimensions of the trunk segment by 10% and
609 20% produced total convex hull volumes of 0.0170 m^3 and 0.0195 m^3, respectively. When
610 convex hull volume was substituted into the OLS predictive equation (Table 8), the body
611 mass of *A. afarensis* was estimated as 20.4 kg (95% prediction interval: 13.5–30.9 kg).
612 Models expanded by 10% and 20% in the trunk region resulted in mass estimates of 23.5 kg
613 (95% predictive interval: 15.5–35.8 kg) and 27.0 kg (95% prediction interval: 17.7–41.0 kg),
614 respectively. Segment inertial properties are not estimated in the present study, but will be
615 incorporated into future multibody dynamic analyses of locomotion.

616

617 **Discussion**

618 The volumetric model of *A. afarensis* (A.L. 288-1) presented here results in an average body
619 mass estimate of 20.4 kg. This figure is lower than several mass estimates published
620 elsewhere for this specimen (Fig. 3), although the sizeable 95% prediction intervals overlap
621 many previous studies and suggest a mass up to 31 kg is statistically supported. When
622 compared with previous studies, the lower average mass estimate calculated here may be
623 consistent with three alternative explanations: (1) that the convex hull predictive model does
624 not work when applied to *A. afarensis*, (2) that the articulated model of A.L. 288-1 is

incorrect, or (3) that the body mass of A.L. 288-1 may have been lower than previously estimated, which are discussed in turn below.

The convex hull predictive model does not work when applied to A. afarensis

Here we have shown that the convex hull mass prediction model performs reasonably well when applied to several modern primate individuals (Table 9), including humans, squirrel monkeys, and a species of night monkey not included in the original training dataset. The convex hulling technique defines a predictable relationship between the overall volume of the skeleton and the amount of soft tissue held beyond its bounds. For convex hulling to underestimate mass therefore, A.L. 288-1 would be required to have held far more soft tissue outside the extent of the convex hull than would characterize a modern primate of similar size.

Many of the modern primate carcasses digitized for the present study were captive individuals rather than wild-caught specimens. The results of Leigh (1994) for anthropoid primates suggest captive body weight is on average 27% higher than non-captive weight. However, captive African apes were not found to be significantly heavier than wild individuals. As these species (alongside humans) are the most relevant taxa for assessing A.L. 288-1, this suggests the use of zoo individuals might not be a factor in the low predicted masses of A.L. 288-1. In contrast, Leigh (1994) also found macaques to be particularly susceptible to obesity, with captive body mass on average 58% above species averages for wild mass. This may go some way to explaining the poor performance of our predictive equation, considerably underestimating the body mass of the captive specimens of *Macaca fuscata* (Table 9). This issue is also highlighted in Figure 7, in which the predictive performance of the convex hull equation is related to the BMI of male humans, with percentage error increasing as a function of BMI. This is unsurprising given the nature of the convex hulling approach, as one assumes a consistent ‘primate-average’ amount of soft tissue to be distributed outside the bounds of the skeleton, and does not account for extreme volumes of adipose tissue. Whilst it is reassuring that humans with a ‘normal’ BMI fall within

653 the range of predictive error expected of the equation, these data are illuminating with
654 regards to the sensitivity of the approach to assumed body composition. Although perhaps
655 less of a problem for primates, this would be an issue for taxa known to undergo
656 considerable seasonal shifts in body composition, such as migratory species.
657 As a 'wild' individual, there is little reason to believe A.L. 288-1 carried unusually
658 large stores of fat above and beyond modern captive primates. Likewise, there is no
659 evidence for *A. afarensis* possessing considerably more muscle beyond the bounds of the
660 skeleton compared to similar sized modern primates, such as the olive baboon (*Papio*
661 *anubis*) included in the training dataset, and muscle attachment sites on the A.L. 288-1
662 skeleton are of comparable prominence to those of other large bodied primates. We
663 therefore consider it unlikely that the low mass estimate presented here is attributable to
664 additional soft tissues that have been unaccounted for in the original convex hull model.
665 It must also be recognized that the modern calibration dataset comprises mostly
666 cadaveric specimens. Whilst the sensitivity analysis conducted above has suggested the
667 inclusion of individuals who have undergone a postmortem does not considerably impact
668 upon estimated masses for A.L. 288-1, it is still the case that our predictive model has not
669 been tested on live non-human primates. Although the equation performs as expected on
670 live humans of normal BMI, further veterinary CT data on non-cadaveric primates would be a
671 welcome future addition. Furthermore, the NCIA human dataset is limited to male patients.
672 Additional whole-body CT data of female subjects may be illuminating with regards to the
673 potential effect of sexual dimorphism on predictive performance.
674
675 *The articulated model of A.L. 288-1 is incorrect*
676 This is almost certainly the case to some extent. Less than half of the skeleton is
677 preserved, and what remains has been subject to taphonomic deformation. A substantial
678 amount of 'sculpting' has been necessary in order to create an articulated model upon which
679 convex hulling can operate. Whilst considerable effort has been made to ensure the
680 reconstruction of damaged/missing elements incorporates the maximum amount of

681 information from existing fragments and is grounded within the context of other closely
682 related taxa, including modern humans, some error is inevitable. Furthermore, due to the
683 volumetric nature of the mass estimate, any errors associated with reconstructing the linear
684 dimensions of missing/damaged skeletal elements become proportionally larger when
685 incorporated into the final volumetric model. Unfortunately, as with any paleontological
686 reconstruction, the degree to which this model accurately reflects the body shape of A.L.
687 288-1 will never be known, though the reconstruction may be corroborated through further
688 finds of fossil skeletons. The more pertinent question then becomes the sensitivity of the
689 convex hulling approach to potential inaccuracies.
690 Here the 'trunk' segment comprises 71% of total convex hull volume of A.L. 288-1,
691 and errors in this region of the body can impact significantly on final body mass estimates.
692 Not only does the 'trunk' consist of many skeletal elements of uncertain articulation
693 (including the pelvis, ribs, and scapulae), the morphology of said elements is frequently
694 contested in the literature, (e.g., Aiello and Dean, 1999). In addition, the trunk region is also
695 one of the poorest in terms of fossil preservation, with ribs being particularly fragile and
696 subject to loss. For this reason, we focused our sensitivity analysis on the effect of overall
697 trunk shape on resulting mass estimates.
698 A height of 1106 mm for A.L. 288-1 agrees with previous estimates of stature
699 (Jungers, 1988a), and the bi-iliac breadth of our 'best-guess' reconstruction overlaps with
700 those published elsewhere (Berge and Goularas, 2010; Ruff, 2010), with both erring on the
701 upper end of previous studies. Yet combined they result in a convex hull mass estimate
702 falling below the majority of other studies (Fig. 3) at 20.4 kg. In contrast, to achieve a mean
703 body mass estimate in excess of 25 kg that is more convergent with previous studies
704 requires the trunk region to be expanded by ~20%, resulting in a bi-iliac breadth of 317 mm,
705 far above the range of values previously considered feasible. In addition, the overall body
706 shape necessary to achieve such high values of body mass appears disproportionally broad
707 in the shoulder and thoracic region (Fig. 9).

Alternative metrics for quantifying 'external body size' including 'stature' (Porter, 1995) or 'stature x body breadth' (Ruff, 1994, 2002) have previously been used to estimate hominin body mass. Such studies have been criticized, however, for involving an additional stage of prediction (estimating stature from preserved long bone lengths and subsequently estimating body mass from stature) and for requiring a considerable portion of the skeleton to be recovered. We must therefore recognize that the convex hulling technique presented here is even more limited in this sense, requiring an entire 3D articulated skeleton to operate on and a non-trivial degree of digital restoration to achieve the model. However, the application of sensitivity analyses in the form conducted above does permit a visual check on body size reconstructions, allowing for the results of linear predictive models (X species weighed Y kg) to be placed into the context of what this means for the body shape of the taxa in question. In this instance, we consider the 20% expanded trunk model to be implausible in the context of hominin body shape, as it would imply that all of the thoracic remains from A.L. 288-1 are taphonomically distorted and result in an even smaller rib cage than in life. This is not particularly feasible given the evidence from KSD-VP-1/1, which suggests a thorax morphology more like the condition found in modern humans. This, however, assumes that the scaling has no effect on thoracic form, and this is an area in which more research needs to be done, for example, through analysis of small bodied modern human populations such as the Andaman Islanders or Khoi-San.

The body mass of A.L. 288-1 may have been lower than previously estimated

As far as the authors are aware, this is the first attempt to estimate the body mass of a fossil hominin using a 3D volumetric technique. That the results presented here for the mass of *A. afarensis* differ quite markedly from those published previously is perhaps unsurprising. Within the wider discipline of paleontology, volumetric reconstructions of fossil birds (Brassey et al., 2013, 2016) and dinosaurs (Henderson, 2006; Sellers et al., 2012) have produced mass estimates lower than traditionally put forward using straightforward linear skeletal dimensions. Interestingly, the study of Porter (1995) perhaps comes closest to

ours in terms of methodology, in which the BMI of A.L. 288-1 was predicted and body mass back-calculated by substituting in a stature of 1050 mm. Porter (1995) estimated a probable mass of 25 kg, and suggested that the values of 28 kg and greater, favored elsewhere, were improbable without the specimen having an extremely high BMI.

Most existing mass estimates of A.L. 288-1 rely upon limb material and produce estimates typically spanning 25–37 kg (Fig. 3). If the low estimates for body mass calculated here are reliable, this would suggest the limb bones of *A. afarensis* were comparatively overbuilt relative to modern humans and apes. Recent evidence has suggested that A.L. 288-1 had relatively more robust limb bone diaphyses compared to articular size (Ruff et al., 2016). Yet the extent to which this translates into the specimen possessing a robust appendicular skeleton relative to total body size can only be understood in the light of non-limb based reconstructions as presented here. Future research may incorporate the results of volumetric mass estimates into further biomechanical analyses of skeletal loading to determine the relative robustness of the skeleton during locomotion.

Conclusions

The method presented here suggests that based on a complete reconstruction of the skeleton, we should expect the body mass of A.L. 288-1 to be 20.4 kg. This is considerably lower than predicted by most published sources although still within the previously published range. This reduction is very much in line with the reductions in body mass estimates seen in other paleontological studies when volumetric approaches are used and may well reflect the fact that A.L. 288-1 is a considerably lighter hominin than has previously been thought. However, it must be remembered that volumetric body masses are particularly sensitive to the reconstruction of the trunk, and the incomplete nature of the preserved ribcage may be the source of this discrepancy in mass estimates. Even so, we would suggest that the heaviest of the previous estimates would require a degree of thorax expansions that would seem unlikely. Of course, this can only be tested when more complete fossils are available.

Whilst convex hulling is a very novel volumetric approach to estimating the mass of A.L. 288-1, there are obvious drawbacks. Not only is the application of convex hulling limited to relatively complete skeletons, but it also requires a modern reference dataset of whole body CT scans, preferably of individuals of known body mass. There are several potential candidates for the future application of volumetric mass estimation to fossil hominin and primate material, however. The Regourdou Neanderthal has a considerable proportion of thoracic material preserved, whilst the *Homo erectus* (WT15000) 'Turkana Boy' is exceptionally complete (albeit immature, thus requiring an ontogenetic reference dataset). Once fully described, the *Australopithecus* 'Little Foot' (Stw 573) may be viable, as will *Homo naledi* (this would currently require a composite, although more complete individuals may be discovered in the future). *Oreopithecus bambolii* (IGF 11778) would require digitization and retrodeformation, but is fairly well represented, likewise *Ardipithecus ramidus* (ARA-VP-6/500), if and when the material becomes publicly available.

Whilst potentially a limiting factor in the past, access to CT facilities is becoming cheaper and more straightforward, and collecting large modern comparative datasets is now entirely feasible. Accessing appropriate cadaveric primate material can indeed be problematic. Yet assuming, as a field, we hold ourselves to the minimum standards and additional best-practices put forward by Davies et al. (2017), the sharing of CT and 3D surface model datasets via online repositories should ensure an ever increasing pool of data to draw from.

Therefore, even in the light of the above limitations, we remain optimistic that volumetric mass estimation has a future role to play in the field of human evolution, most obviously through integration with biomechanical studies of locomotion. And although unlikely to replace traditional linear allometric methods, convex hulling ought to complement such studies wherever possible, as a means of validating the feasibility of mass estimates derived by other approaches. Volumetric reconstructions will also prove particularly useful in exploring the impact of changes in bodily dimensions (pelvis width, ribcage shape) on mass

sets across evolutionary lineages. In particular, future work should explore the possible effects of ontogeny and sexual dimorphism on volumetric body mass estimates.

Acknowledgments

We would like to thank the editor, guest editor, and two anonymous reviewers for their suggested improvements to the manuscript. The authors would like to acknowledge the Kyoto Primate Research Institute (KUPRI), the Visible Human Project, the Cancer Imaging Archive; CARTA, and Morphosource.org for access to datasets. We also thank Doug Boyer (Duke University) for making scans of the A.L. 333 composite skull, and AL288-1 pelvis and sacrum available to us. We acknowledge Andrew Kitchener (National Museum of Scotland, Edinburgh) for providing primate specimens and Martin Baker (University of Liverpool) for conducting CT scanning. We thank Diana Mahoney-Swales for logistical help with arranging the scanning of casts, and Robert Brocklehurst (University of Manchester) for assistance with data management. We also thank C. Owen Lovejoy (Kent State University) for providing a reference model of the A.L. 288-1 pelvis used during preliminary stages and Martin Hauesler for access to his reconstruction of the AL288-1 pelvis. We thank Stephanie Davy-Jow for assistance with some of the preliminary reconstruction, particularly the vertebral column. Data for the vertebral reconstruction were courtesy of Juho Antii-Junno (University of Oulu). Data from Andaman Islanders was collected by T.O'M. with the permission of Robert Kruszynski, Natural History Museum London. Aspects of this work were funded by the Natural Environment Research Council (NE/C520447/1, NE/C520463/1 and NE/J012556/1).

812 **References**

813 Adams, D.C., Otarola-Castillo, E., 2013. Geomorph: an R package for the collection and
814 analysis of geometric morphometric shape data. M. Ecol. Evol. 4, 393–399.
815 Aiello, L.C., Dean, M.C. 1999. An introduction to human evolutionary anatomy. Academic
816 Press, London.
817 Aiello, L.C., Wood, B.A., 1994. Cranial variables as predictors of hominine body mass. Am.
818 J. Phys. Anthropol. 95, 409–426.
819 Alba, D.M., Moyà-Solà, S., Kohler, M., 2003. Morphological affinities of the *Australopithecus*
820 *afarensis* hand on the basis of manual proportions and relative thumb length. J. Hum.
821 Evol. 44, 225–254.
822 Alexander, R.M.N., 1985. Mechanics of posture and gait of some large dinosaurs. Zool. J.
823 Linn. Soc. 83, 1–25.
824 Arnold, C., Matthews, L.J., Nunn, C.L., 2010. The 10kTrees website: a new online resource
825 for primate phylogeny. Evol. Anthropol. 19, 114–118.
826 Asfaw, B., White, T., Lovejoy, O., Latimer, B., Simpson, S., Suwa, G., 1999.
827 *Australopithecus garhi*: a new species of early hominid from Ethiopia. Science 284,
828 629–635.
829 Auerbach, B.M., Ruff, C.B., 2004. Human body mass estimation: a comparison of
830 “morphometric” and “mechanical” methods. Am. J. Phys. Anthropol. 125, 331–342.
831 Barber, C.B., Dobkin, D.P., Huhdanpaa, H., 1996. The quickhull algorithm for convex hulls.
832 ACM T. Math. Software 22, 469–483.
833 Basu, C., Falkingham, P.L., Hutchinson, J.R., 2016. The extinct, giant giraffid *Sivatherium*
834 *giganteum*: skeletal reconstruction and body mass estimation. Biol. Lett. 12,
835 20150940.
836 Bates, K.T., Manning, P.L., Hodgetts, D., Sellers, W.I., 2009. Estimating mass properties of
837 dinosaurs using laser imaging and 3D computer modelling. PLoS One 4, e4532.
838 Bates, K.T., Falkingham, P.L., Macaulay, S., Brassey, C., Maidment, S.C., 2015. Downsizing
839 a giant: re-evaluating *Dreadnoughtus* body mass. Biol. Lett. 11, 20150215.

840 Berge, C., Goularas, D., 2010. A new reconstruction of Sts 14 Pelvis (*Australopithecus*
841 *africanus*) from computed tomography and three-dimensional modeling techniques.
842 J. Hum. Evol. 58, 262–272.

843 Berger, L.R., de Ruiter, D.J., Churchill, S.E., Schmid, P., Carlson, K.J., Dirks, P.H.G.M.,
844 Kibii, J.M., 2010. *Australopithecus sediba*: A New Species of *Homo*-Like Australopith
845 from South Africa. Science 328, 195–204.

846 Braddy, S.J., Poschmann, M., Tetlie, O.E., 2008. Giant claw reveals the largest ever
847 arthropod. Biol. Lett. 4, 106–109.
848 Brassey, C.A., 2017. Body mass estimation in paleontology: A review of volumetric
849 techniques. Paleontol. Soc. Pap. 22, 133–156.
850 Brassey, C. A., Sellers, W. I., 2014. Scaling of convex hull volume to body mass in modern
851 primates, non-primate mammals and birds. PLoS One 9, e91691.
852 Brassey, C.A., Holdaway, R.N., Packham, A.G., Anne, J., Manning, P.L., Sellers, W.I., 2013.
853 More than one way of being a Moa: Differences in leg bone robustness map
854 divergent evolutionary trajectories in Dinornithidae and Emeidae (Dinornithiformes).
855 PLoS One 8, e82668.
856 Brassey, C.A., O'Mahoney, T.G., Kitchener, A.C., Manning, P.L., Sellers, W.I., 2016.
857 Convex-hull mass estimates of the dodo (*Raphus cucullatus*): application of a CT-
858 based mass estimation technique. PeerJ 4, e1432.
859 Bräuer, G., 1988. Osteometrie. In Knußmen, R. (Ed.) Anthropologie: Handbuch
860 der vergleichenden Biologie des Menschen, Volume 1. Gustav Fischer Verlag, Stuttgart.
861 Brown, P., Sutikna, T., Morwood, M.J., Soejono, R.P., Jatmiko, Wayhu Saptomo, E., Awe
862 Due, R., 2004. A new small-bodied hominin from the Late Pleistocene of Flores,
863 Indonesia. Nature 431, 1055–1061.
864 Bush, M.E., Lovejoy, C.O., Johanson, D.C., Coppens, Y., 1982. Hominid carpal,
865 metacarpal, and phalangeal bones recovered from the Hadar Formation: 1974–1977

collections. Am. J. Phys. Anthropol. 57, 651–677.

Cheein, F.A., Guivant, J., 2014. SLAM-based incremental convex hull processing approach for treetop volume estimation. Comput. Electron. Agr. 102, 19–30.

Clark, K., Vendt, B., Smith, K., Freymann, J., Kirby, J., Koppel, P., Moore S., Phillips, S., Maffitt, D., Pringle, M., Tarbox, L., Prior, F., 2013. The Cancer Imaging Archive (TCIA): maintaining and operating a public information repository. J. Digit. Imaging 26, 1045–1057.

Clarke, R.J., 1998. First ever discovery of a well-preserved skull and associated skeleton of an *Australopithecus*. S. Afr. J. Sci. 94, 460–463.

Colbert, E.H., 1962. The weights of dinosaurs. Am. Mus. Novitates 2076, 1–16.

Conroy, G.C., 1987. Problems of body-weight estimation in fossil primates. Intl. J. Primatol. 8, 115–137.

Cook, D.C., Buikstra, J.E., DeRousseau, C., Johanson, D.C., 1983. Vertebral pathology in the Afar australopithecines. Am J. Phys. Anthropol. 60, 83–102.

Crompton, R.H., Weijie, L.Y.W., Günther, M., Savage, R., 1998. The mechanical effectiveness of erect and “bent-hip, bent-knee” bipedal walking in *Australopithecus afarensis*. J. Hum. Evol. 35, 55–74.

Davies, T.G., Rahman, I.A., Lautenschlager, S., Cunningham, J.A., Asher, R.A., Barrett, P.M., Bates, K.T., Bengtson, S., Benson, R.B.J., Boyer, D.M. et al. 2017. Open data and digital morphology. Proc. R. Soc. B. 284, 20170194.

Dingwall, H.L., Hatala, K.G., Wunderlich, R.E., Richmond, B.G., 2013. Hominin stature, body mass, and walking speed estimates based on 1.5 million-year-old fossil footprints at Ileret, Kenya. J. Human Evol. 64, 556–568.

Drapeau, M.S.M., Ward, C.V., Kimbel, W.H., Johanson, D.C., Rak, Y., 2005. Associated cranial and forelimb remains attributed to *Australopithecus afarensis* from Hadar, Ethiopia. J. Human Evol. 48, 593–642.

892 Fariña, R.A., Vizcaíno, S.F., Bargo, M.S., 1998. Body mass estimations in Lujanian (late
893 Pleistocene-early Holocene of South America) mammal megafauna. Mastozool.
894 Neotrop. 5, 87–108.
895 Fleagle, J.G., 2013. Primate adaption and evolution. Academic Press, San Diego, p. 464.
896 Franciscus, R.G., Holliday, T.W., 1992. Hindlimb skeletal allometry in plio-pleistocene
897 hominids with special reference to AL-288-1 (" Lucy"). B. Mém. Soc. Anthropol. Paris.
898 4, 5–20.
899 Garcia-Martinez, D., Barach, A., Recheis, W., Utrilla, C., Torres Sanchez, I., Garcia Rio, R.,
900 Bastir, M., 2014. On the chest size of Kebara 2. J. Hum. Evol. 7, 69–72.
901 Gilad, I. and Nissan, M., 1986. A Study of Vertebra and Disc Geometric Relations of the
902 Human Cervical and Lumbar Spine. Spine 11(2), 154–157
903 Grabowski, M., Hatala, K.G., Jungers, W.L., Richmond, B.G., 2015. Body mass estimates of
904 hominin fossils and the evolution of human body size. J. Human Evol. 85, 75–93.
905 Gregory, W., 1905. The weight of the *Brontosaurus*. Science 22, 572.
906 Gunga, H., Kirsch, K., Baartz, F., Röcker, L., Heinrich, W., Lisowski, W., Wiedemann, A.,
907 Albertz, J., 1995. New data on the dimensions of *Brachiosaurus brancai* and their
908 physiological implications. Naturwissenschaften 82, 190–192.
909 Gunga, H., Kirsch, K., Rittweger, J., Röcker, L., Clarke, A., Albertz, J., Wiedemann, A.,
910 Mokry, S., Suthau, T., Wehr, A., Heinrich, W-D., Shultze, H.P., 1999. Body size and
911 body volume distribution in two sauropods from the Upper Jurassic of Tendaguru
912 (Tanzania). Fossil Rec. 2, 91–102.
913 Gunz, P., Mitteroecker, P., Neubauer, S., Weber, G.W., and Bookstein, F.L., 2009.
914 Principles for the virtual reconstruction of hominin crania. J. Hum. Evol. 57, 48–62.
915 Haile-Selassie, Y., Su, D.G. (Eds.), 2016. The Postcranial Anatomy of Australopithecus
916 afarensis New Insights from KSD-VP-1/1. Springer, Drotrecht.
917 Haile Selassie, Y., Latimer, B.M., Alene, M., Deino, A.L., Gilber, L., Melillo, S.M., Saylor,
918 B.Z., Scott, G.R., and Lovejoy, C.O., 2010a. An early *Australopithecus afarensis*
919 postcranium from Woranso-Mille, Ethiopia. PNAS 107, 12121–12126.

Haile-Selassie, Y., Saylor, B., Deino, A., Alene, M., Latimer, B., 2010b. New hominid fossils from Woranso-Mille (Central Afar, Ethiopia) and taxonomy of early *Australopithecus*. Am. J. Phys. Anthropol. 141, 406–617.

Harris, S., Cresswell, W., Forde, P., Trewhella, W., Woollard, T., Wray, S., 1990. Home-range analysis using radio-tracking data–a review of problems and techniques particularly as applied to the study of mammals. Mamm. Rev. 20, 97–123.

Hartwig-Scherer, S., 1993. Body weight prediction in early fossil hominids: Towards a taxon-"independent" approach. Am. J. Phys. Anthropol. 92, 17–36.

Hauesler, M., Martelli, S.A., Boeni, T., 2002. Vertebrae numbers of the early hominid lumbar spine. J. Hum. Evol. 43, 621–643

Henderson, D., 2006. Burly gaits: Centers of mass, stability, and the trackways of sauropod dinosaurs. J. Vert. Paleo. 26, 907–921.

Hens, S.M., Konigsberg, L.W., Jungers, W.L., 2000. Estimating stature in fossil hominids: which regression model and reference sample to use? J. Hum. Evol. 38, 767–784.

Herrero-Huerta, M., González-Aguilera, D., Rodriguez-Gonzalvez, P., Hernández-López, D., 2015. Vineyard yield estimation by automatic 3D bunch modelling in field conditions. Comput. Electron. Agr. 110, 17–26.

Herridge, V.L, Lister, A.M., 2012. Extreme insular dwarfism evolved in a mammoth. Proc. R. Soc. B. 279, 3193–3200.

Holliday, T.W., Fransiscus, R.G., 2009. Body size and its consequences: Allometry and the lower limb of Liang Bua 1 (*Homo floresiensis*). J. Hum. Evol. 57, 223–228.

Hutchinson, J.R., Ng-Thow-Hing, V., Anderson, F.C., 2007. A 3D interactive method for estimating body segmental parameters in animals: application to the turning and running performance of *Tyrannosaurus rex*. J. Theor. Biol. 246, 660–680.

944 Hutchinson, J.R., Bates, K.T., Molnar, J., Allen, V., Makovicky, P.J., 2011. A computational
945 analysis of limb and body dimensions in *Tyrannosaurus rex* with implications for
946 locomotion, ontogeny, and growth. PLoS One 6, e26037.
947 Jiménez, P., Thomas, F., Torras, C., 2001. 3D collision detection: a survey. Comput. Graph.
948 25, 269–285.
949 Johanson, D., Edey, M.A., 1981. Lucy: The beginnings of humankind. Simon and Schuster,
950 New York.
951 Johanson, D.C., Lovejoy, C.O., Kimbel, W.H., White, T.D., Ward, S.C., Bush, M.E., Latimer,
952 B.M., Coppens, Y., 1982a. Morphology of the Pliocene partial hominid skeleton (A.L.
953 288-1) from the Hadar Formation, Ethiopia. Am. J. Phys. Anthropol. 57, 403–451.
954 Johanson, D.C., Taieb, M., Coppens, Y., (editors). 1982b. Special issue: Pliocene hominids
955 from Hadar, Ethiopia. Am J. Phys. Anthropol. 57, 373–719.
956 Jungers, W.L., 1982. Lucy's limbs: skeletal allometry and locomotion in *Australopithecus*
957 *afarensis*. Nature 297, 676–678.
958 Jungers, W.L., 1988a. Lucy's length: Stature reconstruction in Australopithecus afarensis
959 (A.L. 288-1) with implications for other small-bodied hominids. Am. J. Phys.
960 Anthropol. 76, 227–231
961 Jungers, W.L., 1988b. New estimates of body size in australopithecines. In: Grine, F.E.
962 (Ed.), Evolutionary history of the “robust” australopithecines. Transaction Publishers,
963 New Jersey, pp. 115–125.
964
965 Jungers, W.L., 1990. Problems and methods in reconstructing body size in fossil primates.
966 In: Damuth, J., MacFadden, B.J. (Eds.), Body size in mammalian paleobiology:
967 estimation and biological implications. Cambridge University Press, Cambridge, pp.
968 103–118.

969 Junno, J.-A., Niskanen, M., Nieminen, M.T., Maijanen, H., Niinimäki, J., Bloigu, R.,
970 Tuukkanen, J., 2009. Temporal trends in vertebral size and shape from Medieval to
971 modern-day. PLoS One 4(3), e4836. doi:10.1371/journal.pone.0004836

Kaiser, A., Klok, J., 2008. Do giant claws mean giant bodies? An alternative view on exaggerated scaling relationships. Biol. Lett. 4, 279–280.

Kappelman, J., 1996. The evolution of body mass and relative brain size in fossil hominids. J. Hum. Evol. 30, 243–276.

Kappelman J., Ketcham, R.A., Pearce, S., Todd, L., Akins, W., Colbert, M.W., Feseha, M. Maisano, J.A., Witzel, A., 2016. Perimortem fractures in Lucy suggest mortality from fall out of tall tree. Nature 537, 503-507. doi:10.1038/nature19332.

Kibii, J.M., Churchill, S.E., Schmid, P., Carlson, K.J., Reed, N.D., de Ruiter, D.J., Berger, L.R., 2011. A partial pelvis of *Australopithecus sediba*. Science 333, 1407–1411.

Kimbel, W.H., Johanson, D.C., Rak, Y., 1994. The first skull and other new discoveries of *Australopithecus afarensis* at Hadar, Ethiopia. Nature 368, 449–451.

Konigsberg, L.W., Hens, S.M., Jantz, L.M., Jungers, W.L., 1998. Stature estimation and calibration: Bayesian and maximum likelihood perspectives in physical anthropology. Am. J. Phys. Anthropol. 107, 65–92.

Kramer, P., 1999. Modelling the locomotor energetics of extinct hominids. J. Exp. Biol. 202, 2807–2818.

Kramer, P., Eck, G., 2000. Locomotor energetics and leg length in hominid bipedality. J. Hum. Evol. 38, 651–666.

Kunkel, M.A., Herkommer, M., Reinehr, M., Böckers, T.M., Wilke, H.J., 2011. Morphometric analysis of the relationships between intervertebral disc and vertebral body heights: An anatomical and radiographic study of the thoracic spine. J. Anat. 219, 375–387.

Latimer, B., Ward, C., 1993. The thoracic and lumbar vertebrae. In Walker, A., Leakey, R. (Eds.) The Nariokotome *Homo erectus* skeleton. Berlin, Springer, pp. 267–293.

Latimer, B.M., Lovejoy, C.O., Spurlock, L., Haile-Selassie, Y., 2016. The thoracic cage of KSD-VP-1/1. In: Haile-Selassie, Y., Su, D.F. (Eds.) The Postcranial Anatomy of

997 *Australopithecus afarensis:* New Insights from KSD-VP-1/1. Springer, New York, pp.
998 143–153.
999 Lavin, S.R., Karasov, W.H., Ives, A.R., Middleton, K.M., Garland Jr, T., 2008. Morphometrics
1000 of the avian small intestine compared with that of nonflying mammals: a phylogenetic
1001 approach. Physiol. Biochem. Zool. 81, 526–550.
1002 Leigh, S.R., 1994. Relations between captive and noncaptive weights in anthropoid
1003 primates. Zoo Biol. 13, 21–43.
1004 Leutenegger, W., 1987. Neonatal brain size and neurocranial dimensions in Pliocene
1005 hominids: implications for obstetrics. J. Hum. Evol. 16, 291–296.
1006 Lewin, R., Foley, R.A., 2004. Principles of Human Evolution. Blackwell, London.
1007 Martin, R., Saller, K., 1957. Lehrbuch der Anthropologie. Gustav Fischer, Stuttgart.

1008 Masao, F.T., Ichumbaki, E.B., Cherin, M., Barili, A., Boschian, G., Iurino, D.A., Menconero,
1009 S., Moggi-Cecchi, J., Manzi, G., 2016. New footprints from Laetoli (Tanzania) provide
1010 evidence for marked body size variation in early hominins. eLife 5, e19568.

1011 McHenry, H.M., 1976. Early hominid body weight and encephalization. Am. J. Phys.
1012 Anthropol. 45, 77–83.
1013 McHenry, H.M., 1988. New estimates of body weight in early hominids and their significance
1014 to encephalization and megadontia in “robust” australopithecines. In: Grine, F.E.
1015 (Ed.), Evolutionary history of the “robust” australopithecines. Aldine Transaction, New
1016 Brunswick. pp. 133–48.
1017 McHenry, H.M., 1991. Sexual dimorphism in *Australopithecus afarensis*. J. Human Evol. 20,
1018 21–32.
1019 McHenry, H.M., 1992. Body size and proportions in early hominids. Am. J. Phys. Anthropol.
1020 87, 407–431.
1021 McHenry, H.M., Berger, L.R., 1998. Body proportions in *Australopithecus afarensis* and *A.*
1022 *africanus* and the origin of the genus *Homo*. J. Human. Evol. 35, 1–22.

1023 Meyer, M.R., 2005. Functional biology of the Homo erectus axial skeleton from Dmanisi,
1024 Georgia. PhD Thesis, University of Pennsylvania.
1025 Meyer, M.R., 2016. The Cervical Vertebrae of KSD-VP-1/1. In: Haile-Selassie, Y., Su,
1026 D.F. (Eds.), The Postcranial Anatomy of *Australopithecus afarensis*: New Insights from
1027 KSD-VP-1/1 (Vertebrate Paleobiology and Paleoanthropology). Springer, Dordrecht. Pp.
1028 63–112.
1029
1030 Meyer, M.R., Williams, S.A., Smith, M.P., Sawyer, G.J., 2015. Lucy's back: Reassessment
1031 of fossils associated with the A.L. 288-1 vertebral column. J. Hum. Evol. 85, 174–
1032 180.
1033 Millien, V., Bovy, H., 2010. When teeth and bones disagree: body mass estimation of a giant
1034 extinct rodent. J. Mammal. 91, 11–18.
1035 Nagano, A., Umberger, B.R., Marzke, M.W., Gerritsen, K.G., 2005. Neuromusculoskeletal
1036 computer modeling and simulation of upright, straight-legged, bipedal locomotion of
1037 *Australopithecus afarensis* (A.L. 288-1). Am. J. Phys. Anthropol. 126, 2–13.
1038 Niskanen, M., Junno, J.-A., 2009. Estimation of African apes' body size from postcranial
1039 dimensions. Primates 50, 211–220
1040 Organ, J.M., Ward, C.V. 2006. Contours of the hominoid lateral tibial condyle with
1041 implications for *Australopithecus*. J. Hum. Evol. 51, 113–127.
1042 Polk, J., 2004. Influences of limb proportions and body size on locomotor kinematics in
1043 terrestrial primates and fossil hominins. J. Hum. Evol. 47, 237–252.
1044 Porter, A.M., 1995. The body weight of A.L. 288-1 ('Lucy'): A new approach using estimates
1045 of skeletal length and the body mass index. Int. J. Osteoarchaeol. 5, 203–212.
1046 R Core Team, 2012. R: A language and environment for statistical computing. R Foundation
1047 for Statistical Computing, Vienna.
1048 Robinson, J.T., 1972. Early hominid posture and locomotion. University of Chicago
1049 Press, Chicago.

1050 Rosset, A., Spadola, L., Ratib, O., 2004. OsiriX: an open-source software for navigating in
1051 multidimensional DICOM images. J. Digit. Imaging 17, 205–216.
1052 Ruff, C.B., 1994. Morphological adaptation to climate in modern and fossil hominids. Am. J.
1053 Phys. Anthropol. 37, 65–107.
1054 Ruff, C.B., 2000. Body mass prediction from skeletal frame size in elite athletes. Am. J.
1055 Phys. Anthropol. 113, 507–517.
1056 Ruff, C.B., 2002. Variation in human body size and shape. Annu. Rev. Anthropol. 31, 211–
1057 232.
1058 Ruff, C.B., 2003. Long bone articular and diaphyseal structure in Old World monkeys and
1059 apes. II: Estimation of body mass. Am. J. Phys. Anthropol. 120, 16–37.
1060 Ruff, C.B., 2010. Body size and body shape in early hominins–implications of the Gona
1061 pelvis. J. Hum. Evol. 58, 166–178.
1062 Ruff, C.B., Scott, W.W., Liu, A.Y., 1991. Articular and diaphyseal remodeling of the proximal
1063 femur with changes in body mass in adults. Am. J. Phys. Anthropol. 86, 397–413.
1064 Ruff, C.B., Niskanen, M., Junno, J., Jamison, P., 2005. Body mass prediction from stature
1065 and bi-iliac breadth in two high latitude populations, with application to earlier higher
1066 latitude humans. J. Human Evol. 48, 381–392.
1067 Ruff, C.B., Loring Burgess, M., Ketcham, R.A., Kappelman, J. 2016. Limb bone structural
1068 proportions and locomotor behaviour in A.L. 288-1 (“Lucy”). PLoS One 11,
1069 e0166095.
1070 Ryan, T.M., Sukhdeo, S., 2016. KSD-VP-1/1: Analysis of the postcranial skeleton using
1071 high-resolution computed tomography. In Haile-Selassie, Y. and Su, D.G. (Eds.),
1072 2016. The Postcranial Anatomy of *Australopithecus afarensis* New Insights from
1073 KSD-VP-1/1. Springer, Drotrecht, pp. 39–62
1074 Sanders, W.J., 1998. Comparative morphometric study of the australopithecine vertebral
1075 series Stw-H8/H41. J. Hum. Evol. 34, 249–302.
1076 Schlager, S., 2013. Soft-tissue reconstruction of the human nose - population differences
1077 and sexual dimorphism". PhD Thesis: Albert-Ludwigs-Universität Freiburg

1078 Schmid, P., 1983. Ein Rekonstruktion des Skelettes von A.L. 288-1 (Hadar) und deren
1079 Konsequenzen. Folia Primatol. 40, 283–306.
1080 Schmid, P., Churchill, S.E., Nalla, S., Weissen, E., Carlson, K.J., de Ruiter, D.J., Berger,
1081 L.R., 2013. Mosaic morphology in the thorax of *Australopithecus sediba*. Science
1082 340, 1234598.
1083 Sellers, W.I., Dennis, L.A., Wang, W.J., Crompton, R.H., 2004. Evaluating alternative gait
1084 strategies using evolutionary robotics. J. Anat. 204, 343–351.
1085 Sellers, W.I., Cain, G.M., Wang, W., Crompton, R.H., 2005. Stride lengths, speed and
1086 energy costs in walking of *Australopithecus afarensis*: using evolutionary robotics to
1087 predict locomotion of early human ancestors. J. R. Soc. Interface 2, 431–441.
1088 Sellers, W.I., Hepworth-Bell, J., Falkingham, P., Bates, K., Brassey, C., Egerton, V.,
1089 Manning, P.L., 2012. Minimum convex hull mass estimations of complete mounted
1090 skeletons. Biol. Lett. 8, 842–845.
1091 Simpson, S.W., Spurlock, L.B., Lovejoy, C.O., Latimer, B., 2010. A new reconstruction of the
1092 KNM-WT 15000 juvenile male pelvis. Am. J. Phys. Anthropol. 141(Suppl. 50), 189.
1093 Spocter, M.A., Manger, P.R., 2007. The use of cranial variables for the estimation of body
1094 mass in fossil hominins. Am. J. Phys. Anthropol. 134, 92–105.
1095 Squyres, N., Ruff, C.B., 2015. Body mass estimation from knee breadth, with application to
1096 early hominins. Am. J. Phys. Anthropol. 158, 198–208.
1097 Smith, R.J., 1994. Regression models for prediction equations. J. Hum. Evol. 26, 239–244.
1098 Smith, R.J., 2002. Estimation of body mass in paleontology. J. Hum. Evol. 43, 271–287.
1099 Smith, R.J., 2009. Use and misuse of the reduced major axis for line-fitting. Am. J. Phys.
1100 Anthropol. 140, 476–486.
1101 Stein, K., Csiki, Z., Rogers, K.C., Weishampel, D.B., Redelstorff, R., Carballido, J.L.,
1102 Sander, M., 2010. Small body size and extreme cortical bone remodeling indicate
1103 phyletic dwarfism in *Magyarosaurus dacus* (Sauropoda: Titanosauria). PNAS. 107,
1104 9258–9263.

1105 Steudel-Numbers, K.L., 2006. Energetics in *Homo erectus* and other early hominins: the
1106 consequences of increased lower-limb length. J. Hum. Evol. 51, 445–453.
1107 Sutton, M., Rahman, I., Garwood, R., 2014. Techniques for virtual palaeontology. John
1108 Wiley and Sons, Chichester.
1109 Symonds, M.R.E., Blomberg, S.P., 2014. A primer on phylogenetic generalized least
1110 squares. In Garamszegi, L.Z. (Ed.) Modern phylogenetic comparative methods and
1111 their application to evolutionary biology. Springer-Verlag, Berlin. p. 552.
1112 Syväranta, J., Lensu, A., Marjomäki, T.J., Oksanen, S., Jones, R.I., 2013. An empirical
1113 evaluation of the utility of convex hull and standard ellipse areas for assessing
1114 population niche widths from stable isotope data. PLoS One 8, e56094.
1115 Tague, R.G., 1989. Variation in pelvic size between males and females. Am. J. Phys.
1116 Anthropol. 80, 59–71.
1117 Tague, R.G., Lovejoy, C.O., 1986. The obstetric pelvis of A.L. 288-1 (Lucy). J. Hum. Evol.
1118 15, 237–255.
1119 Treece, G.M., Prager R.W., Gee. A.H., 1999 Regularised marching tetrahedra: improved
1120 iso-surface extraction. Comp. Graph. 23, 583–598.
1121 Trinkaus, E., Ruff, C.B., 2012. Femoral and tibial diaphyseal cross-sectional geometry in
1122 Pleistocene *Homo*. Paleoanthropol. 2012, 13–62
1123 Vančata, V., 2005. A preliminary analysis of long bone measurements of *Homo floresiensis*:
1124 bone robusticity, body size, proportions and encephalisation. Anthropologie 43, 173–
1125 182.
1126 Wang, W., Crompton, R.H., Carey, T.S., Günther, M.M., Li, Y., Savage, R., Sellers, W.I.,
1127 2004. Comparison of inverse-dynamics musculo-skeletal models of A.L. 288-1
1128 *Australopithecus afarensis* and KNM-WT 15000 *Homo ergaster* to modern humans,
1129 with implications for the evolution of bipedalism. J. Hum. Evol. 47, 453–478.
1130 Williams, S.A., Russo, G.A., 2015. Evolution of the Hominoid vertebral column: The long and
1131 the short of It. Evol. Anthropol: Issues News and Reviews 24(1):15-32

1132 Williams, S.A., Russo, G.A., 2016. The fifth element (of Lucy's sacrum): Reply to Machnicki,
1133 Lovejoy, and Reno. Am J Phys Anthropol 161(2), 374–378.
1134 Williams, S.A. Ostrofsky, K.R., Frater, N., Churchill,S.E., Schmid,P., Berger, L.R. 2013. The
1135 vertebral column of *Australopithecus sediba.* Science 340(6129),1232996
1136 Williams, S.A., Middleton, E.R., Vilamil, C.I., Shattuck, M.R., 2016. Vertebral numbers and
1137 human evolution Am. J. Phys. Anthropol. 159(S61):S19-S36
1138 Zollikofer, C.P.E., Ponce de León, M., 2005. Virtual Reconstruction: A Primer in Computer-
1139 Assisted Paleontology and Biomedicine. Wiley, London.

Figure legends

Figure 1. The convex hulling technique. A) Series of 500 points located in 2D space, B) the 26 outermost points defining the convex hull are highlighted in red, C) the convex hull (red line) represents the minimum volume polygon that may be fitted around the data whilst remaining convex, D) a larger point cloud of ~160,000 points based on the isosurface of a *Macaca* skull, with 136 outermost points contributing to the form of the convex hull.

Figure 2. The convex hulling approach applied to the Olive baboon (*Papio anubis*). Left) Isosurface of the skeleton extracted from the CT scan; Right) Closed manifold convex hulls around the extremities of the skeletal functional units, from which minimum skeletal volume is calculated.

Figure 3. Predicted body mass for *Australopithecus afarensis* (A.L. 288-1) over time. Where upper and lower bounds are included in a publication, they are represented by two data points. Mass estimates sourced from: Johansen and Edey (1981); Jungers (1982, 1988b, 1990); Leutenegger (1987); McHenry (1988, 1991, 1992); Franciscus and Holliday (1992); Hartwig-Scherer (1993); Porter (1995); Ruff (2010); Squryres and Ruff (2015); Grabowski et al. (2015). Note, some of the above studies may incorporate previously published raw data or mass estimates into their own analyses, and as such may be non-independent. Values represent extreme upper and lower mass estimates of a given publication and do not necessarily reflect the authors' preference for which values may be most appropriate (see text). Points in red represent results of the present study.

Figure 4. Pelvis reconstruction. Left top, Cranial view, Right top, medial view, Left bottom, posterior view, Right bottom, anterior view.

Figure 5. Complete articulated model of A.L. 288-1 upon which convex hulling and mass estimation was conducted. Left, anterior view; right, lateral view.

Figure 6. A) Convex hull predictive model, in which $\log_{10}$ total convex hull volume (m^3) is plotted against $\log_{10}$ body mass (kg). Line fitted using ordinary least squares (see Table 5 for details of the fitted equation). B) Primate consensus phylogeny sourced from 10kTrees (http://10ktrees.fas.harvard.edu/) used as a basis for phylogenetically corrected phylogenetically generalized least squares regression.

Figure 7. The relationship between percentage prediction error of the convex hull equation and body mass index (BMI) when applied to male humans. Green = 'healthy' BMI, yellow = 'overweight' BMI, red = 'obese' BMI. BMI calculated as mass(kg)/height(m)^2.

Figure 8. The complete *Australopithecus afarensis* reconstruction with convex hulls fitted.

Figure 9. A sensitivity analysis of the effect of uncertainty in the size of the trunk region upon body mass estimates. From left to right; original articulated trunk model (light blue), trunk expanded 10% in dorsoventral and mediolateral extent (green), trunk expanded 20% in dorsoventral and mediolateral extent (purple).

Table 1. A range of mass estimates derived for A.L. 288-1 based upon various skeletal elements.[a]

	Predicted body mass (kg)	
Skeletal element	**All Hominoidea**	***Homo sapiens***
Humeral head	17.4	27.3
Elbow	16.5	30.7
Radial head	12.9	28.2
Thoracic vertebra 12	24.1	32.5
Sacrum	28.5	17.0
Femoral head	27.9	27.9
Femoral shaft	35.2	37.1
Proximal tibia	32.2	27.8
Distal tibia	27.1	24.4
Talus	37.0	27.6

[a] Values taken from McHenry (1992) for ordinary least squares regression models. For definitions of the dimensions measured from each skeletal element, see McHenry (1992). The data highlight the sensitivity of the traditional bivariate mass estimation approach to the skeletal element upon which the predictive model is based.

Table 2. Convex hull specimen list and calculated convex hull (qhull) volumes.[a]

Species	Common name	Source	Body mass (kg)	qhull Volume (m^3)
Homo sapiens	Human	NLM	68.9	4.91×10^{-2}
Pongo pygmaeus	Orangutan	-	45.0	3.25×10^{-2}
Pan troglodytes	Chimpanzee	-	50.9[b]	4.18×10^{-2}
Gorilla gorilla	Gorilla	KUPRI	176.0	9.57×10^{-2}
Hylobates lar	Lar gibbon	KUPRI	6.65[b]	6.60×10^{-3}
Hylobates agilis	Agile gibbon	KUPRI	6.75	5.40×10^{-3}
Saimiri sciureus	Squirrel monkey	KUPRI	0.759	6.00×10^{-4}
Macaca fuscata	Japanese macaque	KUPRI	6.60	5.10×10^{-3}
Chlorocebus aethiops	Grivet monkey	KUPRI	3.78	3.70×10^{-3}
Hylobates pileatus	Pileated gibbon	NMS	7.40	4.95×10^{-3}
Alouatta caraya	Black howler monkey	NMS	5.40	3.31×10^{-3}
Trachypithecus cristatus	Silvery langur	NMS	7.50	3.83×10^{-3}
Cebus apella	Brown capuchin	NMS	1.56	1.15×10^{-3}
Leontopithecus rosalia	Golden lion tamarin	NMS	0.425	3.18×10^{-4}
Papio anubis	Olive baboon	NMS	15.0	1.23×10^{-2}

[a] NLM = National Library of Medicine, KUPRI = Kyoto University Primate Research Institute, NMS = National Museum of Scotland.

[b]Body mass estimated on the basis of radial surface area derived from CT scans, using a previously published predictive equation derived from extant Hominoids (Ruff, 2003). Note

that 11 of the 15 individuals included have body masses of less than 15 kg, and thus fall considerably below the likely body mass of A.L. 288-1.

Table3

Table 3. Obstetric dimensions and indices of pelvic reconstruction compared with other female fossil and extant hominin pelves.[a]

	A.L. 288-1 *Au. afarensis* This reconstruction	A.L. 2881 *Au. afarensis*	MH2 *Au. sediba*	STS15 *Au. africanus*	BSN49P27 *Homo sp.*	*H. sapiens*		*P. troglodytes*	
						Mean	S.D.	Mean	S.D.
Bi-iliac breadth (BIB)	264	268.3*	250	256.3	288	259.5	16.4	122.4	18.3
Bi-acetabular diameter (BAD)	114.1	118*	122.3	107.5	131	123.2	6.5	105.8	35.6
BIB/BAD	1.96	2.27	2.04	2.38	2.2	2.1	0.13	1.16	
Inlet SD	80	76	81.7	83	98	105.2	19.1	143.7	12.6
Inlet TD	128.5	132	117.6	116.8	124.5	131.6	10.4	100	12.3
Inlet SD/TD index	62.3	57.6	69.5	71.1	78.7	80	17.4	146.1	20.1
Midplane SD	103.6	-	97.9	-	-	125.1	16	137.5	26.8
Outlet SD	85.8	71	97.4	-	-	119.4	17.8	122.4	9.6
Subpubic angle	77°	81°	76°	107.2°	110°	89.6°	12.3°	-	-

[a] All A.L. 288-1 measurements are from Tague and Lovejoy (1986) except (*), which were absent from this publication. These are therefore taken from Berge and Goularas (2010) (who measured Schmid's (1983) reconstruction of A.L. 288-1). BSN49P27 dimensions are from

Simpson et al. (2010). *Homo sapiens* measurements from Tague (1989). MH2, STS15, and *Pan troglodytes* from Kibii et al. (2011).

SD=Saggital Diameter, TD = Transverse Diameter

Table 4. Additional measurements of the pelvic reconstruction.[a]

Dimension	Measurement (mm)
Midplane saggital diameter	97.1
False pelvis transverse diameter	255.7
Midplane posterior space	71.2
Outlet posterior space	88.0
Midplane anterior space	77.5
Sacral breadth	86.4
Total sacral height	73.8

[a] All measurements following Tague (1989), except total sacral height.

Table 5. Measurements of long bones of A.L. 288-1.[a]

Element	Length (mm)
Ulna	223
Radius	203
Tibia	247
Fibula	225
Femur	280
Clavicle	104
Humerus	237

[a]All elements are from the right side apart from the femur, which has been mirrored. Measurements are from reconstructed scans (femur, tibia) and 3D prints of reconstructions (all others).

Table6

Table 6. Posterior vertical heights (in mm) of vertebral bodies in *Homo sapiens*, *Pan troglodytes*, *Australopithecus afarensis, Australopithecus africanus, Australopithecus sediba*, and *Homo erectus.*[a]

Sample	Vertebra	C1	C2	C3	C4	C5	C6	C7	T1	T2	T3	T4	T5	T6	T7	T8	T9	T10	T11	T12	L1	L2	L3	L4	L5
Andaman[(1)]	*n*	-	-	8	7	7	9	8	7	9	9	9	9	9	9	8	9	9	7	7	8	9	10	10	10
	Body height	-	-	10.21	10.23	10.64	10.78	11.91	14.05	15.10	15.29	15.24	16.02	16.28	17.44	17.49	17.96	19.32	21.05	22.35	22.25	23.67	23.76	23.16	21.32
	Body height SD	-	-	1.12	1.22	1.10	1.04	0.91	1.09	1.25	1.28	1.45	1.38	1.57	1.39	1.42	1.17	1.99	1.99	2.04	2.27	1.81	1.69	1.99	3.29
Homo sapiens[(2)]	*n*	-	23	23	23	23	23	23	23	23	23	23	23	23	23	23	23	23	23	23	23	23	23	23	23
	Body height	-	**36.91**	**11.64**	**11.59**	**12.38**	**12.32**	**13.31**	**16.59**	**17.45**	**17.45**	**18.55**	**18.69**	**19.28**	**20.29**	**20.67**	**21.90**	**22.30**	**23.92**	**24.97**	**26.24**	**26.37**	**25.95**	**25.77**	**23.90**
	Body height SD	-	1.81	1.29	1.05	1.16	1.23	2.14	1.48	1.67	1.39	1.85	2.12	2.25	1.61	2.37	2.14	2.25	2.32	2.15	2.67	2.30	2.63	2.08	2.61
Pan troglodytes[(3)]	*n*	25	25	25	25	25	25	25	25	25	25	25	25	25	25	25	25	25	25	25	25	25	25	25	-
	Body height	33.75	11.53	11.91	12.23	12.71	12.54	13.64	14.91	15.61	15.49	15.44	15.75	15.58	15.61	15.69	16.10	17.25	18.79	21.46	25.60	26.52	26.44	26.42	-
	Body height SD	4.27	2.79	2.04	1.89	2.16	2.02	2.07	1.95	1.75	2.24	2.12	2.19	2.10	2.12	1.76	2.04	2.10	2.68	2.68	2.95	3.30	3.31	3.17	-
A.L. 288.1[(4)]		-	-	-	-	-	-	-	-	-	-	-	-	13.3	-	13.6	p	14.4	16.1	p	-	-	21.6	-	-
A.L. 288.1[(5)]		-	-	-	-	-	-	-	-	-	-	-	-	13.3	13.6	p	14.4	16.1	p	-	-	p	21.6		
STS14[(6)]		-	-	-	-	-	-	-	-	-	12.3	12.8	13.3	13.6	14	14.6	15.4	16.8	19.1	19.6	19.9	19.5	19.1	17.3	16.8
MH1[(7)]		-	-	-	-	-	-	-	-	-	-	-	-	-	-	-	-	-	-	-	17.1	-	15.7	-	-
MH2[(7)]		-	-	-	-	-	-	-	-	-	-	-	11.5	12.5	-	-	-	-	-	-	-	-	-	21.5	17.4
STW 431[(8)]		-	-	-	-	-	-	-	-	-	-	-	-	-	-	-	-	-	-	-	23.9	24.3	23.9	22.5	19.8
STW8/41[(8)]		-	-	-	-	-	-	-	-	-	-	-	-	-	-	-	-	-	-	-	24.8	24.4	23.2	-	19
SK853/3981[(8)]		-	-	-	-	-	-	-	-	-	-	-	-	-	-	-	-	-	-	-	-	15.2	-	-	-
KSDVP1/1[(8)]		-	-	11.4	13.6	13.8	13.1	-	-	-	-	-	-	-	-	-	-	-	-	-	-	-	-	-	-
KNMWT15000[(9)]		-	-	-	-	-	-	8.7	1.5	11.4	11.6	-	11.8	12.7	12.8	-	-	-	15.5	-	17.3	19.7	17.1	15.8	14.9
Dmanisi[(10)]		6.9	29.9/14.74	12.7	-	-	-	-	-	-	17.2	-	-	-	-	-	-	-	24	-	-	26.6	-	-	-

[a] This measurement is defined as M2, posterior vertebral body height in Brauer (1998) after Martin and Saller (1957). SD refers to standard deviation. [(1)] This paper; [(2)] from Junno et al. (2009); [(3)] from Niskanen and Junno (2009); [(4)] original from Johansen et al. (1982); [(5)] positions after Meyer et al. (2015); [(6)] from Robinson (1972), using Hauesler et al.'s (2002) corrected positions; [(7)] after Williams et al. (2013), thoracic and cervical heights measured from scans, this paper; [(8)] after Meyer (2016); [(9)] after Latimer and Ward (1993); [(10)] D2673, D2721, D2715, D2672, from Meyer (2005) and Mayer et al. (2015).

Table 7. Reconstructed spine heights using proportions from modern comparative samples.[a]

Sample	Predicted vertebral column height (mm)
STS14 and *Homo sapiens* (Dry)	340.5
STS14 and *Pan troglodytes* (Dry)	369.1
AL288-1 and *Pan troglodytes* (Dry)	346.0
Homo sapiens (Blackgate) (Dry)	330.0
Homo sapiens (Blackgate) (Wet)	415.4
Homo sapiens (Andaman) (Dry)	339.8
Homo sapiens (Andaman) (Wet)	422.3

[a] The equation used for dry "height" = ((∑ 〖vertebralbodyheighAL288-1〗)/(% contribute of bones to column height))×100 height = $\left(\frac{\sum vertebralbodyheighAL288-1}{\%\ contribute\ of\ bones\ to\ column\ height}\right) \times 100$

For estimation of intervertebral disc heights, the values given in Gilad and Nissan (1986) and Kunkel et al. (2011) were scaled to the resulting predicted heights of each vertebra, excepting the surviving vertebrae, where the original values were substituted.

Table 8. Ordinary least squares (OLS), reduced major axis (RMA), and phylogenetic generalized least squares (PGLS) regressions of log_{10} total convex hull volume (m^3) against log_{10} body mass (kg).[a]

Fit	a	a±95%	b	b±95%	r^2	%SEE
OLS	3.17	3.02-3.33	1.02	0.95-1.09	0.988	20.3
RMA	3.19	3.04-3.34	1.03	0.96-1.09	0.988	13.8
PGLS	3.32	2.96-3.67	1.07	0.94-1.20	*	25.5

[a] ±95% = 95% confidence intervals of the slope and intercept, %SEE = percentage standard error of the estimate. %SEE on logged data OLS regression was calculated as 10^(log_{10}(100)+SEE)). %SEE for RMA regression was based on residuals calculated according to Organ and Ward (2006).

*The OLS definition of r^2 does not easily carry over to PGLS. Rather than reporting a 'pseudo r^2', we err on the side of caution and do not report r^2 (Symonds and Blomberg, 2014).

Table9

Table 9. Modern primate specimens used to test the accuracy of the convex hull (qhull) predictive equation.[a]

Species	Common name	Source	Accession number	Sex	BMI	Body mass (kg)	qHull volume (m^3)	qHull mass (kg)	% difference
Aotus trivirgatus	Three striped night monkey	KUPRI	1322	M		1.03	8.31×10^{-4}	1.06	2.81%
Saimiri sciureus	Squirrel monkey	KUPRI	287	M		0.62	4.32×10^{-4}	0.54	13.3%
Saimiri sciureus	Squirrel monkey	KUPRI	283	M		0.71	6.37×10^{-4}	0.81	13.4%
Saimiri sciureus	Squirrel monkey	KUPRI	280	M		0.86	6.51×10^{-4}	0.83	4.40%
Macaca fuscata	Japanese macaque	KUPRI	897	F		4.50	2.57×10^{-3}	3.36	29.0%
Macaca fuscata	Japanese macaque	KUPRI	369	F		10.2	5.86×10^{-3}	7.77	27.0%
Homo sapiens	Human	TCIA	NaF-PROSTATE-01-0005	M	21.4	68.7	4.93×10^{-2}	69.5	1.14%
Homo sapiens	Human	TCIA	NaF-PROSTATE-01-0007	M	24.0	82.2	5.20×10^{-2}	73.4	10.7%
Homo sapiens	Human	TCIA	NaF-PROSTATE-01-0009	M	24.4	90.1	5.43×10^{-2}	76.8	14.8%
Homo sapiens	Human	TCIA	NaF-PROSTATE-01-0003	M	26.9	82.5	4.57×10^{-2}	64.4	21.9%

Homo sapiens	Human	TCIA	NaF-PROSTATE-01-0002	M	29.2	91.5	4.72×10^{-2}	66.6	27.2%
Homo sapiens	Human	TCIA	NaF-PROSTATE-01-0006	M	31.7	88.5	4.28×10^{-2}	60.2	32.0%

[a] In one instance, the predictive model overestimated live body mass, whilst in three instances the model underestimated live model mass.

TCIA = The Cancer Imaging Archive; BMI = body mass index, calculated as mass(kg)/height(m)^2. M = male; F = female.

Table 10. Segmental convex hull (qhull) volumes calculated for the articulated model of *Australopithecus afarensis.*[a]

Body segment	**qhull Volume (m^3)**
Skull	0.001175
Neck	0.000140
Trunk	0.010573
+10% trunk	0.012794
+20% trunk	0.015225
Upper arm	0.000179
Lower arm	0.000117
Hand	0.000233
Thigh	0.000530
Shank	0.000299
Foot	0.000111
Total volume including trunk	0.014826
Total volume including +10% trunk	0.017047
Total volume including +20% trunk	0.019478

[a]Values for limb segments refer to one side of the body only.

Figure1

Click here to download high resolution image

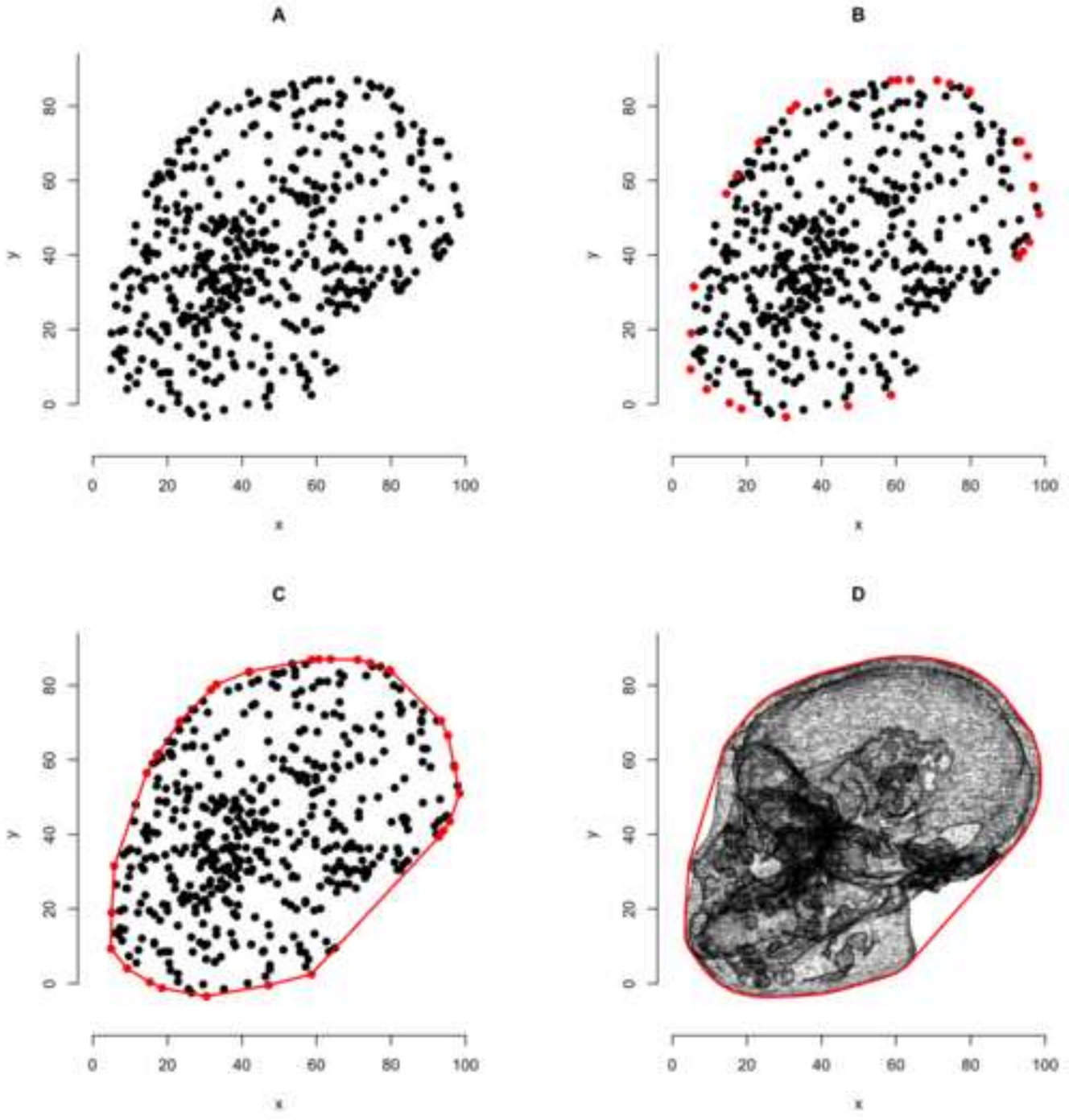

Figure2

Click here to download high resolution image

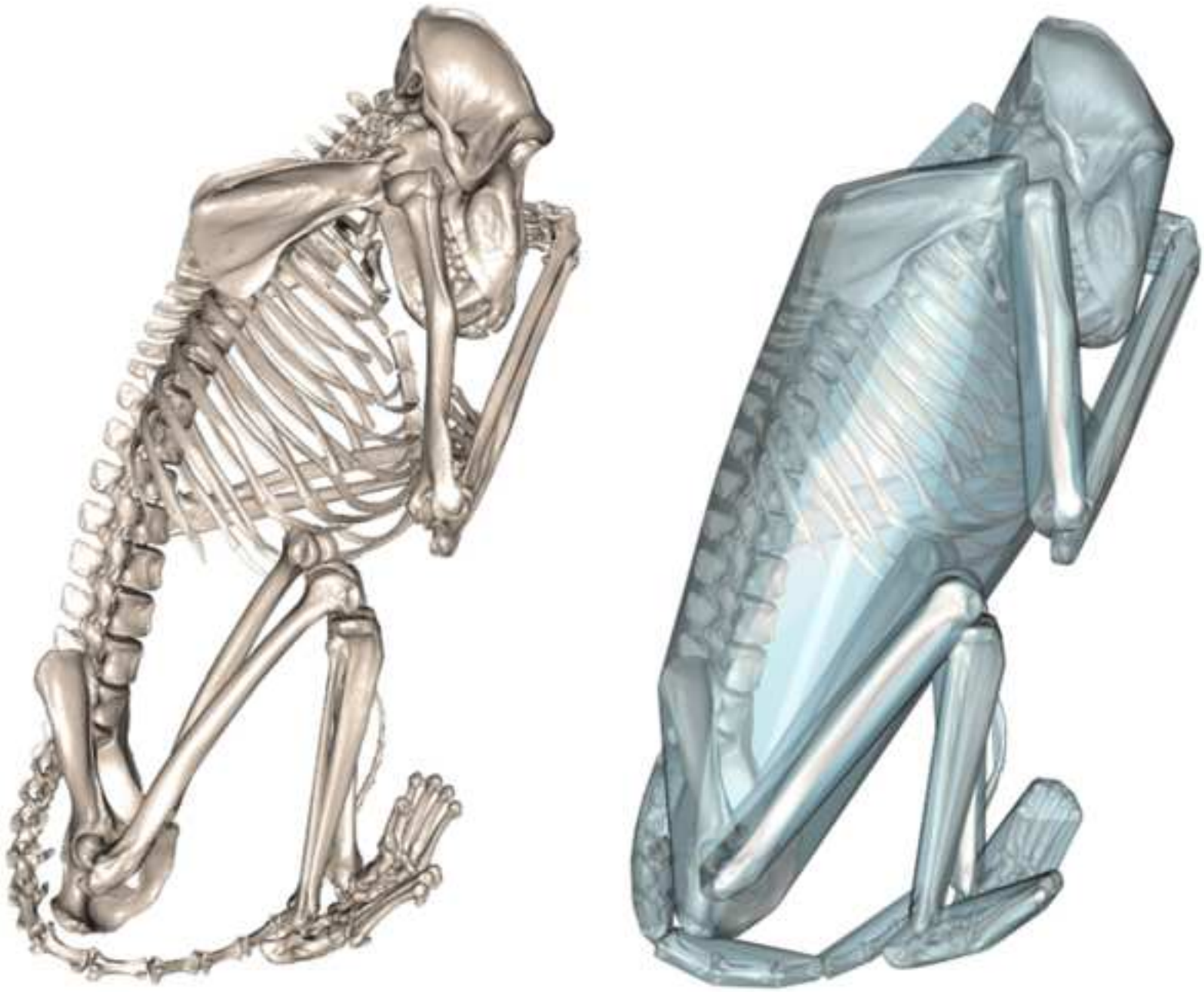

Figure3
Click here to download high resolution image

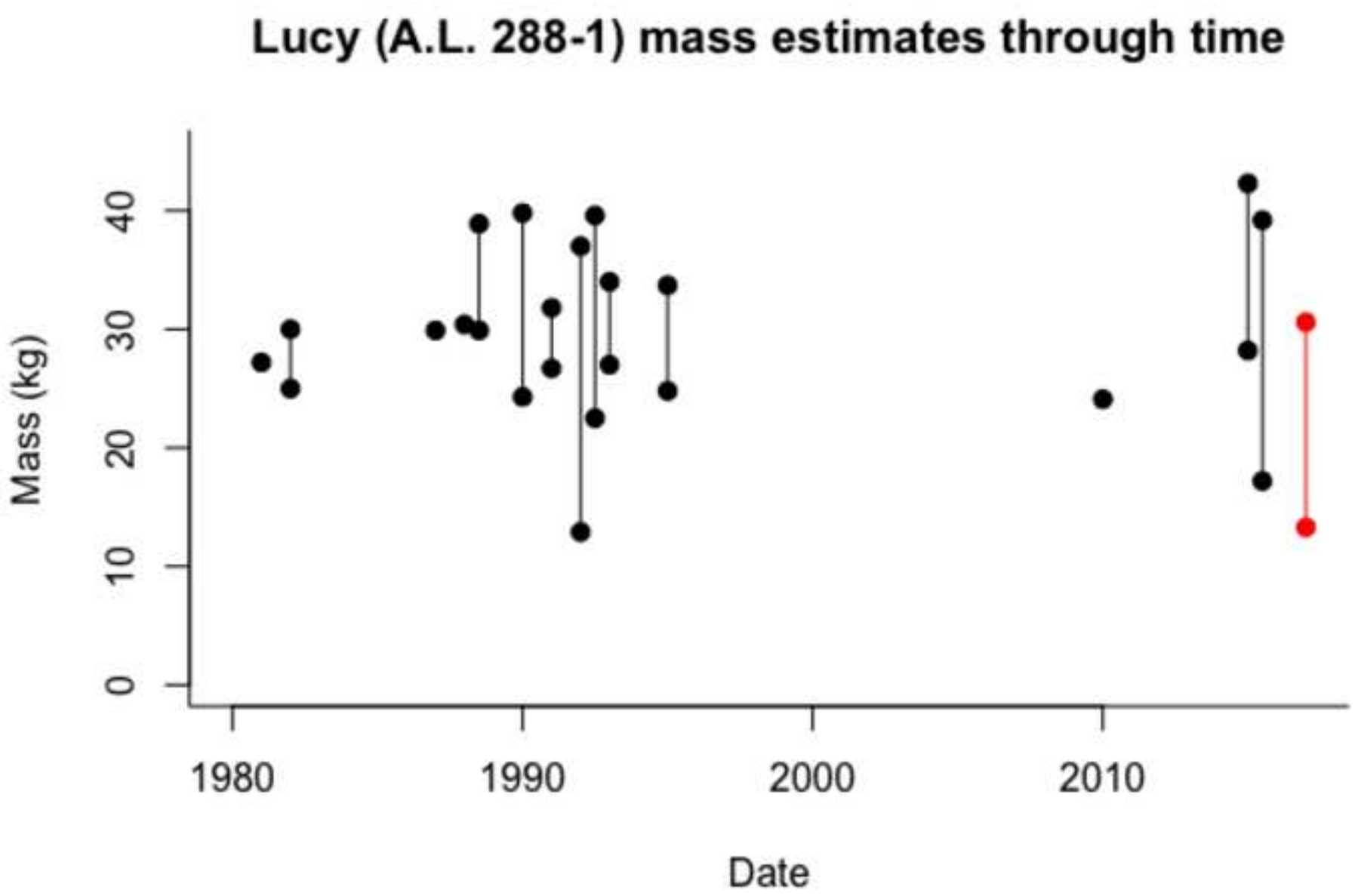

Figure4

Click here to download high resolution image

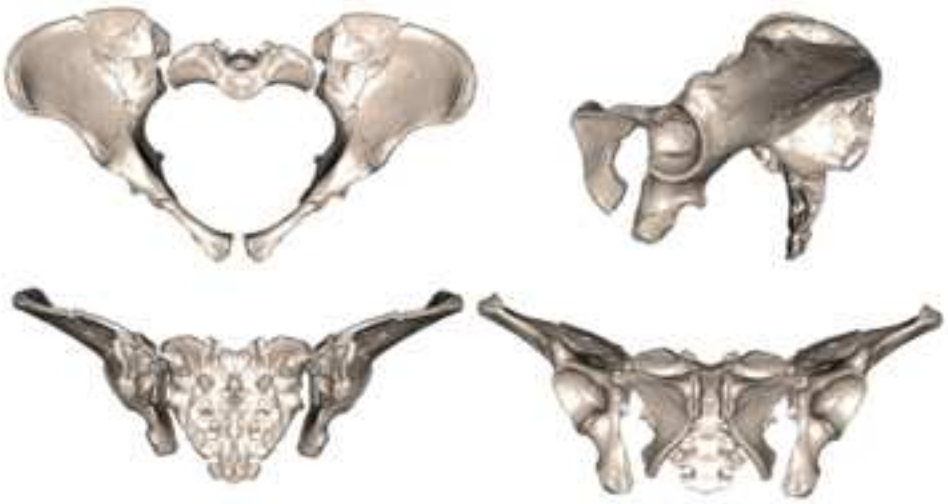

Figure5
Click here to download high resolution image

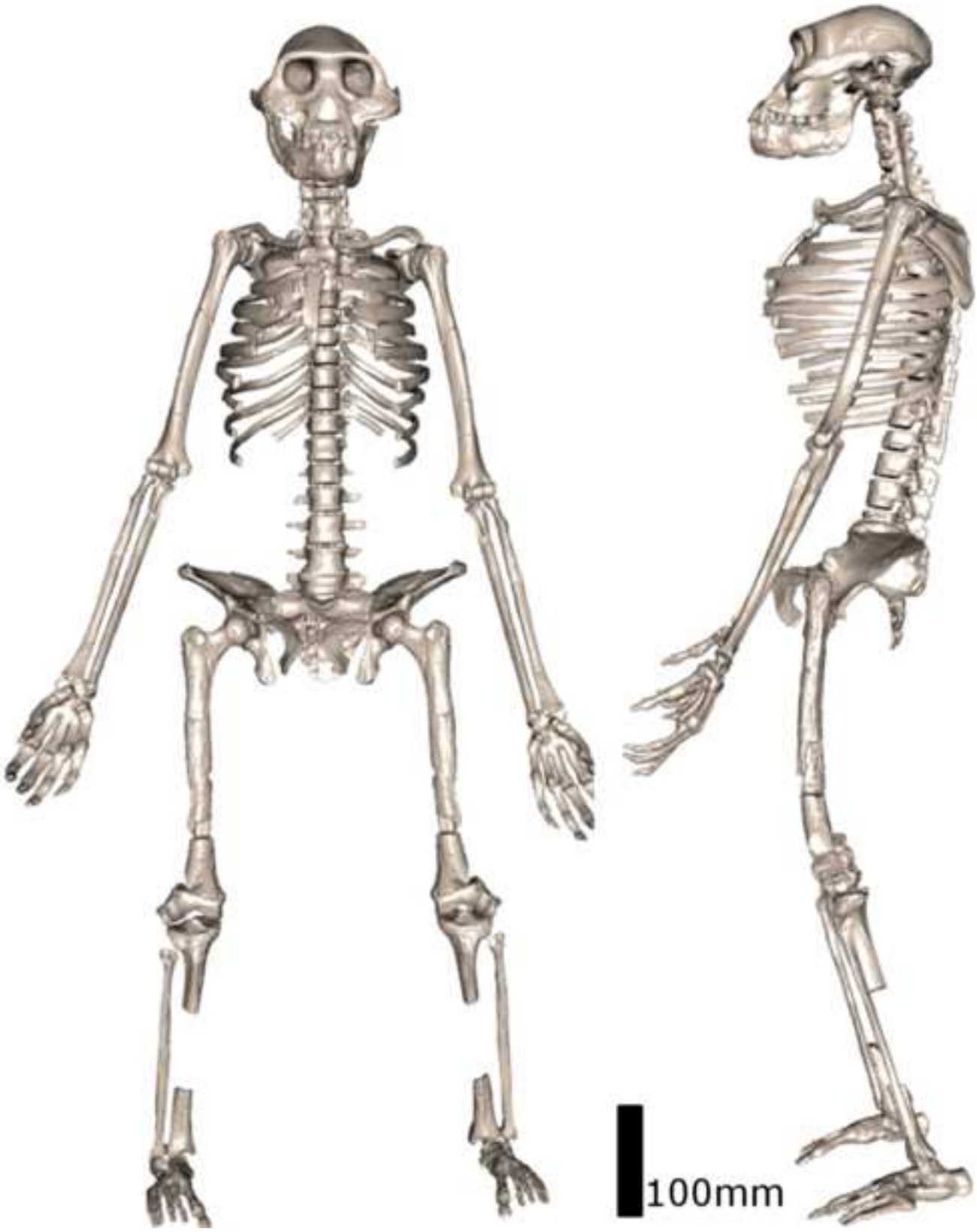

Figure6

Click here to download high resolution image

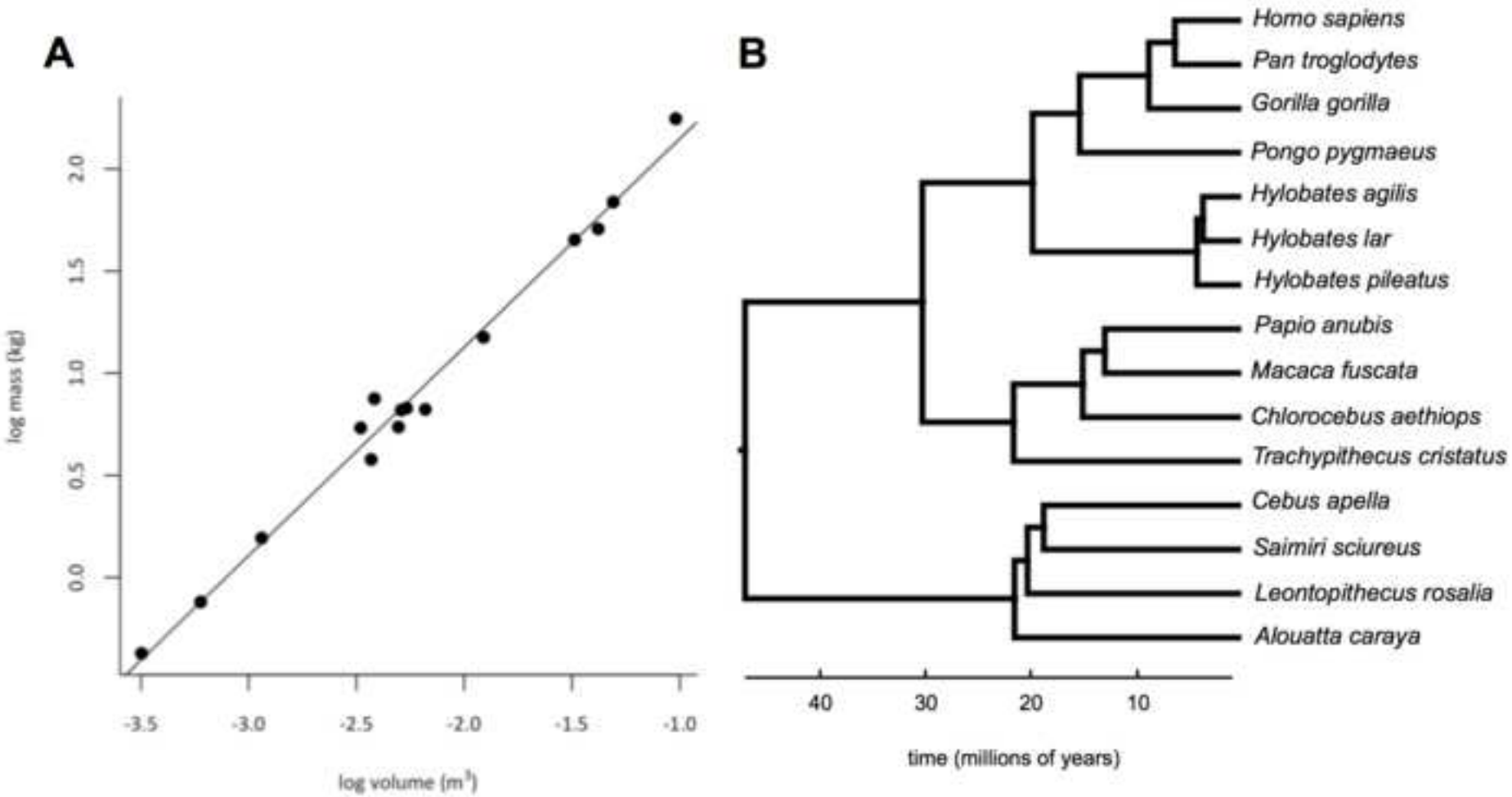

Figure7

Click here to download high resolution image

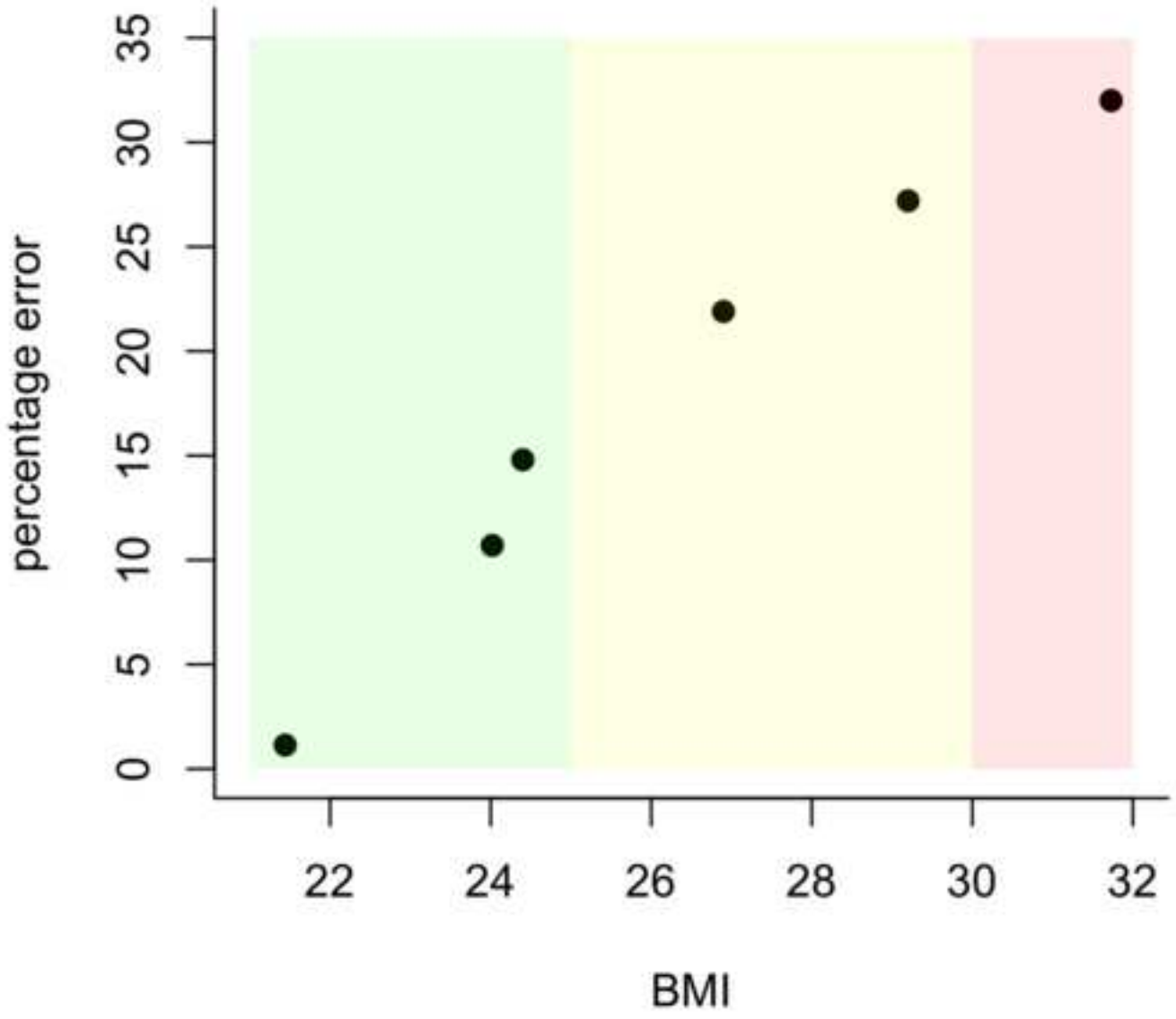

Figure8

Click here to download high resolution image

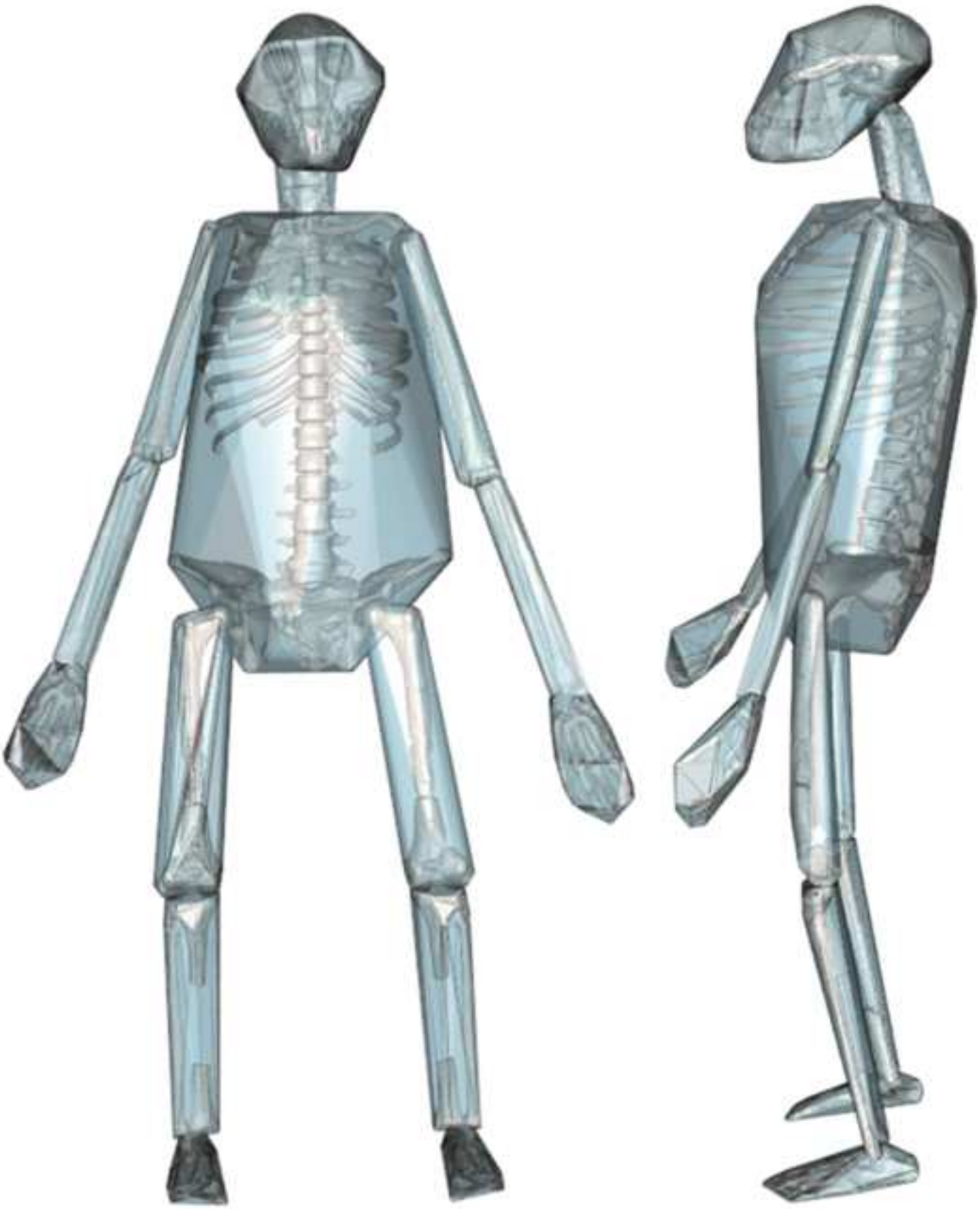

Figure9

Click here to download high resolution image

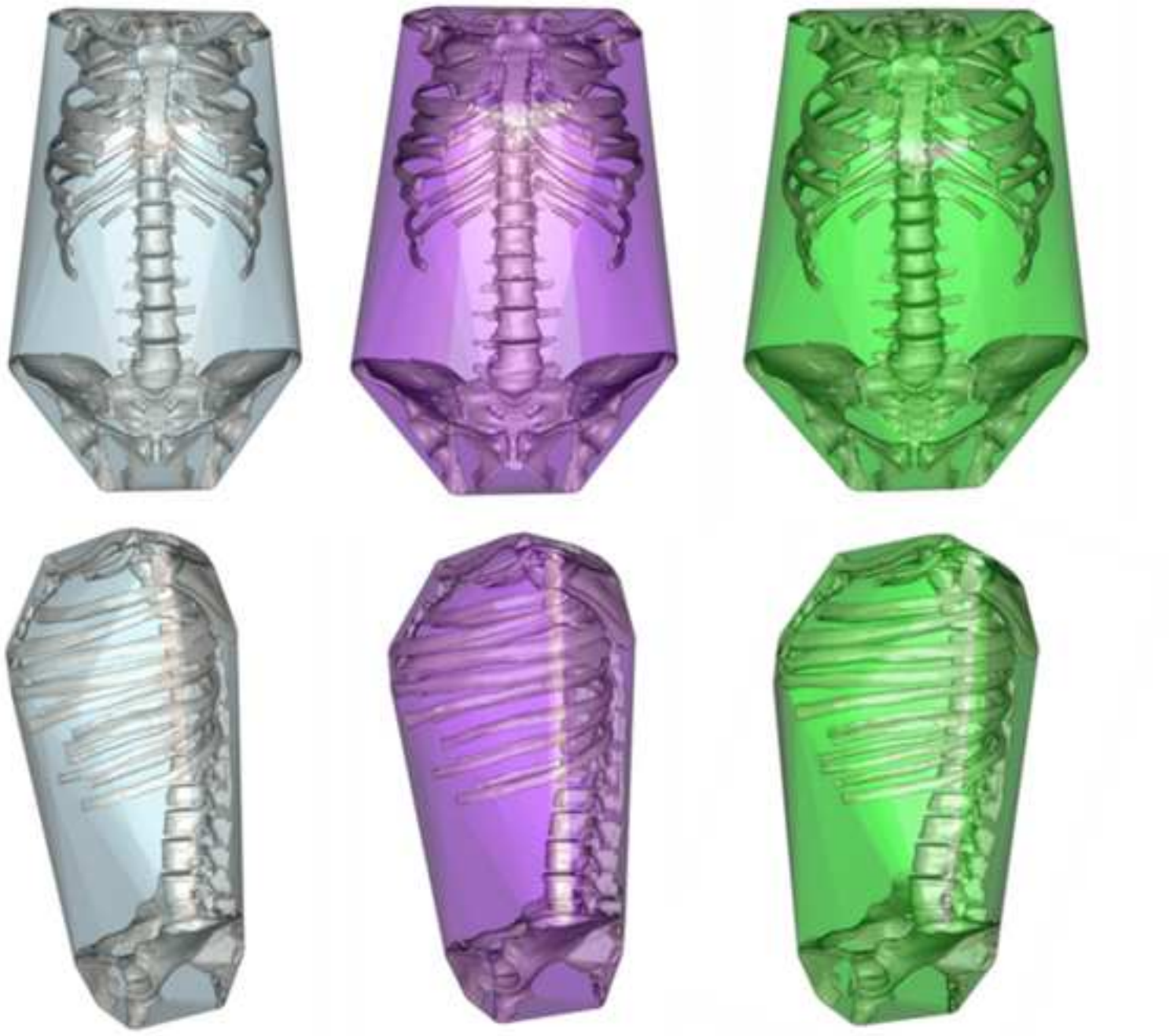

Supplementary Material

Click here to download Supplementary Material: SupplementaryMaterial merged-done.docx